

**Potential Influence of a Midlatitude Oceanic Frontal Zone on the Annular Variability in
the Extratropical Atmosphere as Revealed by Aqua-Planet Experiments**

by

Takeaki SAMPE^{*},

Research Center for Advanced Information Science and Technology, University of Aizu,

Aizu-Wakamatsu, Japan

Hisashi NAKAMURA[†],

Department of Earth and Planetary Science, University of Tokyo, Tokyo, Japan

Atsushi GOTO,

Office of International Affairs, Japan Meteorological Agency, Tokyo, Japan

The special issue on the Aqua-Planet Experiment Project, *Journal of Meteorological Society
of Japan*

Aug. 13, 2010, submitted.

Mar. 2, 2011, revised.

^{*} Corresponding author: Takeaki Sampe, Research Center for Advanced Information Science and Technology, University of Aizu, Tsuruga, Ikki-machi, Aizu-Wakamatsu, 965-8580 Japan. Email: sampe@u-aizu.ac.jp

[†] Current affiliation: Research Center for Advanced Science and Technology, University of Tokyo, Japan; Also affiliated with Research Institute for Global Change, JAMSTEC, Yokohama, Japan.

Abstract

Potential influence of a midlatitude SST frontal zone on the zonally symmetric variability in the extratropical atmosphere is assessed through idealized aqua-planet experiments with a general circulation model. In one experiment with a midlatitude frontal SST gradient as sharp as that observed in the Southwestern Indian Ocean, the annular mode is well reproduced in the model summer hemisphere. As actually observed in the Southern Hemisphere, the model annular mode represents a north-south seesaw in westerly wind speed around the climatological joint axes of a midlatitude westerly jet and storm track, with intensified (weakened) midlatitude westerlies under the enhanced (reduced) eddy momentum transport. This essential feature of the annular mode is retained also over the winter hemisphere, although its structure is somewhat distorted owing to the seasonal intensification of a subtropical jet (STJ). In the other experiment, elimination of the frontal SST gradient results in an equatorward shift of westerly wind anomalies associated with the annular mode in the summer hemisphere, in step with a shift of the mean joint axes of the jet and storm track. More importantly, both the amplitude and persistence of the mode are substantially reduced. In the winter hemisphere, the elimination also results in a marked weakening of the annular variability of midlatitude westerlies. Due to the weakening of the near-surface baroclinicity from lack of the frontal SST gradient, anomalous eddy momentum transport is also reduced markedly. Unlike the observed annular mode, the dominant mode of variability primarily represents STJ variability. Though idealized, these model experiments suggest the potential importance of a midlatitude oceanic frontal zone for the year-round dominance and robustness of the annular mode signal against the wintertime intensification of a STJ, by enhancing storm-track activity.

1. Introduction

Zonally symmetric variability of the extratropical atmosphere has been a research topic for a long time. Particularly, variations in the midlatitude zonal-mean westerlies have been known as “zonal index cycle” (e.g., Rossby 1939; Namias 1950; Lorenz 1951). In the Southern Hemisphere (SH), the zonally symmetric variability accounts for a larger fraction of the total intraseasonal variability than in the Northern Hemisphere (NH), owing to higher zonal symmetry in the SH surface conditions. The SH “annular” variability has therefore been investigated in a number of studies (e.g., Kidson 1988; Karoly 1990; Hartmann and Lo 1998) since reliable atmospheric data became available for the SH. The dominant mode of the SH annular variability is characterized by a meridional dipole of zonal wind anomalies that represents north-south migrations of a polar-front jet (PFJ) about its time-mean axial position at $\sim 50^{\circ}\text{S}$ (Limpasuvan and Hartmann 2000). Essentially the same mode of variability is identified as the leading mode of geopotential height or sea-level pressure (SLP) variability, corresponding to a seesaw of air mass between the polar and midlatitude regions (Thompson and Wallace 2000). This SH “annular mode” (SAM) bears certain similarities in its spatial structure to the leading mode of variability in zonal-mean SLP or zonal winds ($[U]$; the brackets denote zonal averaging) over the NH, called the NH annular mode (NAM; Thompson and Wallace 2000) or “Arctic Oscillation” (Thompson and Wallace 1998). There are nevertheless some noticeable differences between the NAM and SAM in their seasonality and the role of transient eddies. The $[U]$ variance associated with the NAM is stronger by a factor of three in winter months than in summer months, while the corresponding seasonality is much weaker in the SAM-associated $[U]$ variance (Limpasuvan and Hartmann 2000). Furthermore, the seasonality is also weaker in the structure of the SAM-associated $[U]$ anomalies within the troposphere (Hartmann and Lo 1998), despite pronounced seasonal variations in the intensity of a subtropical jet (STJ; Nakamura and Shimpo 2004).

The $[U]$ variations associated with the annular modes are forced by anomalous eddy

fluxes, but the characteristics of eddy fluxes are different between the NAM and SAM. High-frequency transients contribute mostly to the eddy forcing on the SAM (Karoly 1990; Hartmann and Lo 1998; Codron 2007), while stationary eddies make a greater contribution to the NAM variability (DeWeaver and Nigam 2000; Limpasuvan and Hartmann 2000; Kimoto et al. 2001). Activity of high-frequency transient eddies tends to be organized into “storm tracks” over the midlatitude oceans. The annular modes accompany anomalies in both the storm-track activity and PFJ that are closely related to one another, especially in the SH due to the weakness of stationary waves (Lorenz and Hartmann 2001). The relationship between the variability of a midlatitude jet stream (i.e., PFJ) and that of a storm track has been investigated also with simple models and atmospheric general circulation models (AGCMs) (e.g., Robinson 1991, 2006; Yu and Hartmann 1993; Feldstein and Lee 1996; Limpasuvan and Hartmann 2000). Overall, the observational and modeling studies have shown that the SAM-associated $[U]$ variations result from their interaction with transient eddies. Yu and Hartmann (1993), for example, suggested that transient eddies tend to be deformed so as to transport more (less) westerly momentum poleward when a midlatitude jet migrates poleward (equatorward). In addition, a midlatitude storm track tends to migrate meridionally following the PFJ, leading to the anomalous convergence of eddy westerly momentum transport (e.g., Kidson and Sinclair 1995). These processes act to maintain the anomalous westerly jet (Yoden et al. 1987; Shiogama et al. 2004). Poleward eddy heat flux tends to fluctuate in conjunction with the anomalous upper-level eddy activity associated with the SAM, acting to accelerate surface $[U]$ in the same direction as upper-level $[U]$ anomalies (Limpasuvan and Hartmann 2000). Through an analysis of temporal characteristics of SAM-associated anomalies in $[U]$ and eddy forcing, Lorenz and Hartmann (2001) suggested positive feedback between them, which acts to prolong extreme events of the SAM.

Linear theories of baroclinic instability (e.g., Charney 1947; Eady 1949) indicate that transient eddy activity is sensitive to the thermal structure of the troposphere. Traditionally,

the zonal-mean thermal structure has been considered to be determined in balance between differential radiative heating and meridional heat transport by atmospheric eddies (cf. baroclinic adjustment; Stone 1978). In recent years, however, the importance of oceanic influences on midlatitude storm tracks has been pointed out recently. For example, Nakamura and Shimpo (2004) pointed out that the core regions of the SH storm track and PFJ are collocated all year round with the core of the Antarctic Polar Frontal Zone (APFZ), a prominent oceanic frontal zone in the Indian Ocean extending almost zonally around 45~50°S. They suggested that particularly strong eddy activity in the storm-track core is sustained by the enhanced near-surface baroclinicity associated with sharp SST gradients across the APFZ, as confirmed by an AGCM experiment by Inatsu and Hoskins (2004). Nakamura et al. (2004) discussed the significance of the close association observed among a storm track, PFJ and midlatitude oceanic front, to postulate a new conceptual model of the atmospheric general circulation in which the role of sharp SST gradients in a midlatitude oceanic frontal zone is emphasized in anchoring a storm track and attendant PFJ. Nakamura et al. (2008) and Sampe et al. (2010) further verified this close association through AGCM experiments with different SST profiles prescribed as the model lower boundary condition. In their experiments, elimination of frontal SST gradients led to substantial weakening of transient eddy activity and a westerly PFJ in midlatitudes, shifting the lower-tropospheric mean westerly axis equatorward. They suggested that the existence of the oceanic frontal zone could be of critical importance for the atmospheric general circulation in the extratropics, particularly in anchoring a storm track and thereby maintaining a PFJ. The influence of SST gradients on the mean field of transient eddy activity and westerly jets has also been addressed in Brayshaw et al. (2008) and Chen et al. (2010). It is therefore conjectured that the presence of such a prominent oceanic front as APFZ may significantly influence the annular modes of atmospheric variability by shaping the mean state of a storm track and PFJ. However, oceanic influences upon the annular modes of atmospheric variability through transient eddy forcing

have not been investigated in depth.

The objective of this study is to examine how midlatitude frontal SST gradients can influence the low-frequency annular variability of the PFJ and associated transient eddy activity, especially in the SH. Due to a higher degree of zonal symmetry of the surface conditions in the SH, stationary waves and their forcing on the annular modes are much weaker than in the NH. Therefore, the essential dynamics of the SAM can be elucidated through simulations of simple models or idealized AGCMs (e.g., Robinson 1991, 2006; Feldstein and Lee 1996). The influence of midlatitude oceanic frontal zones for the SH annular variability can be revealed in the purest manner in “aqua-planet” AGCM experiments in which the model lower boundary is entirely set to be the ocean with zonally uniform SST prescribed. Though leading to the loss of such a feature observed in the SH as the planetary waves forced by Antarctica, this idealized experimental setting is nevertheless useful for clarifying the role of the oceanic frontal zones in the annular variability of the extratropical atmosphere through a comparison of experiments with and without realistic frontal SST gradients in the model boundary condition.

The experimental design, including the prescribed SST profiles, is given in Section 2. Influences of a midlatitude oceanic frontal zone on low-frequency variations of the zonal-mean westerlies and transient eddy activity is examined in Section 3, and annular modes simulated in the AGCM and influences of the oceanic frontal zone on them are examined in Section 4. Discussion and concluding remarks are addressed in Section 5. The experimental design is almost the same as that in Sampe et al. (2010), and the reader can refer to it for a more detailed description of the model and the significant role of midlatitude oceanic fronts for the mean state of the atmosphere. In addition to some of the results of our experiments highlighted in Nakamura et al. (2008), we provide more comprehensive analyses in the following sections.

2. Experimental design

We used an AGCM called AFES (AGCM for the Earth Simulator; Ohfuchi et al. 2004, 2007), which includes standard physical parameterization schemes with resolution of the triangular truncation at the total wavenumber of 79 with 48 sigma levels (T79 L48). The horizontal resolution is equivalent to about 1.5° in latitude and longitude on the regular grid. This resolution is sufficient for resolving sharp SST gradients in the major midlatitude frontal zones as observed in the South Indian Ocean. In our “aqua-planet” setting, no landmass was given at the model lower boundary, where the prescribed SST fields were zonally uniform. We adopted two different meridional profiles of SST: hereafter referred to as the “CTL” and “NF” profiles (Fig. 1). The CTL profile is based on the climatology for the period 1982-1995 observed in the southwestern Indian Ocean¹, where the core region of the SH storm track is observed throughout the year (Nakamura and Shimpo 2004). The minimum SST was set to be 0°C to exclude effects of sea ice from our experiment². It is characterized by a frontal SST gradient around latitude 45° in each of the hemispheres. In the NF profile this sharp SST gradient was eliminated and replaced by a relaxed, uniform gradient of $0.3^\circ\text{C}/110\text{km}$ for the model SH and $0.35^\circ\text{C}/110\text{km}$ for the NH (Fig. 1). The SST profile observed in austral summer (December-January-February) was prescribed for the model NH, and that in austral winter (June-July-August) for the SH. The model NH (SH) thus corresponds to the summer (winter) hemisphere. Correspondingly, insolation was fixed to the boreal summer solstice condition.

In order to examine low-frequency variability, we performed the integration of the

¹ The SST dataset is NOAA Optimum Interpolation SST V2, available at <http://www.esrl.noaa.gov/psd/data/gridded/data.noaa.oisst.v2.html> .

² Due to the absence of sea ice, the surface baroclinicity observed along the ice edge around Antarctica was not prescribed in our experiments. However, the midlatitude storm track is observed far off the ice edge in the South Indian Ocean (Nakamura and Shimpo 2004). The ice-free condition also implies the surface temperature assigned in the polar regions was warmer than observed.

AGCM over a 60-month period after a 6-month spin-up period. The model output was sampled every six hours. Sub-weekly fluctuations of a given variable associated with transient eddies have been extracted through a digital high-pass filter with the half-power cutoff period of 8 days. To extract low-frequency variability, U and eddy statistics (e.g., variance of meridional wind fluctuations $v'v'$, meridional fluxes of westerly momentum $u'v'$ and sensible heat $v'T'$) at any grid point have been 8-day low-pass filtered for the following analyses.

Figure 2 shows the climatological-mean SLP distributions in the individual hemispheres for the CTL and NF experiments. In each of the hemispheres, the SLP field displays circumpolar patterns with a high-pressure belt in the subtropics and a low-pressure belt in high latitudes. The high degree of zonal symmetry in SLP confirms the statistical stability of zonal averaging. As evident in Fig. 3, the differences in the time-mean $[U]$ and transient eddy activity between the CTL and NF experiments shown in Sampe et al. (2010) were well reproduced in our 60-month statistics. In the summer hemisphere (i.e., the model NH), the axis of a westerly PFJ is located at 49° latitude in the CTL experiment, while it is shifted about 10° equatorward in the NF experiment as a response to the elimination of the frontal SST gradient in midlatitudes (Figs. 3a and 3b). The elimination results in marked weakening of baroclinic eddy growth (recognized as 850-hPa $[v'T']$ in Fig. 3e) and a reduction in upper-level eddy amplitude (recognized as 250-hPa $[v'v']$ in Fig. 3c). Consequently, the poleward eddy transport of westerly momentum is also reduced markedly (250-hPa $[u'v']$ in Fig. 3d), leading to the weakening of the eddy-driven PFJ and the associated equatorward shift of its axis. In the winter hemisphere (i.e., the model SH), an intense STJ forms in the subtropical upper troposphere in both the CTL and NF experiments (Fig. 3a). The elimination of the frontal SST gradient results in the diminution of a PFJ, with a decrease and an increase in westerly wind speed in midlatitudes and the subtropics, respectively (Figs. 3a and 3b), in a manner consistent with the reduced poleward transport of westerly momentum and sensible heat by transient eddies (Figs. 3d and 3e). In the CTL

experiment, a low-level storm track is anchored near the midlatitude SST frontal zone not only in the summer hemisphere but also in the winter hemisphere (Fig. 3e), although free-tropospheric baroclinicity is greatest below the winter STJ (Figs. 3a and 3b). This result suggests a significant influence of the SST frontal zone on the storm track formation. More details of the mean state for these experiments can be found in Sampe et al. (2010).

3. Low-frequency variability simulated in the aqua-planet experiments

a) Zonal-mean wind

Figures 4a and 4b show low-frequency variance of $[U]$ at the 250 and 925 levels ($[U_{250}]$ and $[U_{925}]$), respectively, for our experiments. The cosine of latitude was multiplied to the variance to represent the latitudinal dependence of the grid area. None of the variance maxima is found to coincide with the mean position of any westerly jet stream (cf. Figs. 4a-b and 3a-b). Rather, the variance of the summertime $[U_{250}]$ is minimized at the mean PFJ axis and maximized at its equatorward and poleward flanks in each of the CTL and NF experiments, representing meridional migrations of the PFJ axis. In the NF experiment, the elimination of the midlatitude frontal SST gradient results in a marked reduction in the summertime $[U_{250}]$ variance and an equatorward shift of its maxima and minimum by $\sim 10^\circ$ in latitude (Fig. 4a), in harmony with a dramatic reduction in eddy statistics and the equatorward shift of the time-mean axes of the PFJ and storm track (Fig. 3). Compared to the $[U_{250}]$ statistics, the variance of $[U_{925}]$ is much less, especially in the subtropics, and its local minimum is closer to the mean westerly axis in each of our experiments. The two maxima of the $[U_{925}]$ variance and its minimum in between are all shifted equatorward in the NF experiment (Fig. 4b) as in the upper troposphere.

In the winter hemisphere, the variance of $[U_{250}]$ peaks at the poleward flank of the mean PFJ axis, at the equatorward flank of the mean STJ core and between these jet streams in the CTL experiment. In the NF experiment, the variance decreases markedly in

midlatitudes (by $\sim 60\%$ at 55°S compared to the CTL experiment; Fig. 4a), where mean transient eddy activity is also weakened substantially (by $\sim 40\%$ in amplitude of the 250-hPa meridional wind velocity; Fig. 3c) as a consequence of the elimination of the midlatitude frontal SST gradient. The decrease in the midlatitude $[U]$ variance is also pronounced at the 925-hPa level. These results are suggestive of a close association between the low-frequency $[U]$ variability and transient eddy activity in the extratropics.

In the summer hemisphere of the CTL experiment, the mean PFJ axis (at latitude of $\sim 50^\circ$; see Figs. 3a and 3b.) almost coincides with a local midlatitude minimum in the $[U_{925}]$ variance (Fig. 4b), whereas the variance is particularly large poleward of the mean PFJ axis. These features are consistent with the meridional distribution of the surface $[U]$ variance actually observed in the SH, which is characterized by a distinct peak at 60°S , poleward of the mean PFJ ($\sim 50^\circ\text{S}$) and a secondary peak at 40°S (Thompson and Wallace 2000).

b) Storm tracks

Figures 4c-e show the variance of the low-frequency fluctuations in zonal-mean statistics of transient eddies, including their meridional fluxes of westerly momentum and sensible heat. In the winter hemisphere, the low-frequency variability in the upper-level eddy activity measured as rms in the 250-hPa eddy meridional wind velocity $[v'_{250}{}^2]^{1/2}$ is maximized around the midlatitude storm-track axis at 49°S , very close to the PFJ axis (cf. Fig. 3). In the summer hemisphere, the variability peaks slightly equatorward of the mean storm-track axis. The presence of the midlatitude frontal SST gradient augments not only the time-mean storm-track activity but also its low-frequency variability in both the upper and lower troposphere. In fact, the variability in the midlatitude eddy activity is weaker in the NF experiment (Fig. 4c). Likewise, the low-frequency variability in 850-hPa poleward eddy heat flux $[v'T'_{850}]$ is much weaker in the NF experiment (Fig. 4e). In the CTL experiment, the low-frequency variability in $[v'T'_{850}]$ has a distinct peak slightly equatorward of the mean

low-level storm-track axis defined as the maximum in the time-mean $[v'T'_{850}]$ in each of the hemispheres. Compared to the NF experiment, the low-frequency variability in the 250-hPa meridional eddy transport of westerly momentum $[u'v'_{250}]$ is also enhanced markedly (more than doubled) in the CTL experiment in each of the hemispheres, with a peak at the joint axes of the mean PFJ and storm track (Fig. 4d). In the NF experiment (Fig. 4d), the peak of the variability is shifted equatorward.

It is noteworthy that a particular degree of variability, defined as the ratio of low-frequency rms of a given eddy statistic to its long-term mean, is especially large for the poleward eddy flux of westerly momentum $[u'v'_{250}]$, which is important as eddy forcing on low-frequency $[U]$ variability. In the CTL experiment, the largest time-mean value of midlatitude $[u'v'_{250}]$ is 45 (60) $\text{m}^2 \text{s}^{-2}$ and the corresponding value of its low-frequency rms is 27 (28) in the winter (summer) hemisphere. The particular degree of variability is thus about 60% (45%), substantially higher than its counterparts for the eddy heat flux $[v'T'_{850}]$ and upper-level eddy amplitude $[v'_{\text{rms} 250}]$. The degree of variability for $[v'T'_{850}]$ is 25~30% for each of the hemispheres.

The influence of the midlatitude oceanic frontal zones and strong upper-level jets on the meridional migration of a storm track is manifested in the instantaneous position of a storm-track axis. Figure 5 shows the frequency or “probability density”³ distribution of the instantaneous axis of the primary storm track. The axis was identified every 6 hours for each of the hemispheres based on a given zonal-mean eddy statistic, and the frequency of the presence of the instantaneous axis was then counted for each latitudinal grid over the entire data period (i.e., 1800 days). In the CTL experiment, the lower-tropospheric storm-track axis, defined as the latitude of the instantaneous maximum in $[v'T'_{850}]$, shows a strong tendency to

³ Strictly speaking, the quantities shown in Fig. 5 are not identical to the probability density because of the slight dependence of the latitudinal intervals of the model Gaussian grid on its latitude, but the dependence is practically negligible.

be anchored in the vicinity of the midlatitude SST frontal zone. The upper-level storm-track axis, defined as the maximum $[v'_{\text{rms}}]_{250}$, exhibits a similar tendency. In the NF experiment, in contrast, the wintertime lower-tropospheric storm-track axis is broadly distributed from the subtropics to subpolar latitudes with a much less distinct peak than in the CTL experiment (Fig. 5c), in the absence of any strong anchoring effect under the relaxed SST gradient. The primary axis of the upper-level storm track forms not only in midlatitudes but also in the subtropics, the latter of which appears to manifest the trapping effect of eddies by the strong STJ (Fig. 5a; Nakamura and Sampe 2002). In the CTL experiment, by contrast, the primary axis of the wintertime upper-level storm track exhibits little preference along the STJ (Fig. 5a). In the summer hemisphere, the storm track exhibits strong preference for staying around the mean PFJ axis at latitudes of $\sim 49^\circ$ and $\sim 41^\circ$ in the CTL and NF experiment, respectively (Figs. 5b and 5d), in good correspondence to the mean latitudinal distribution of eddy amplitude. As the STJ is weak in the summer hemisphere, the storm track is almost always organized around the PFJ axis in both the CTL and NF experiments.

The comparison between Figs. 4 and 5 suggests that, in acting to anchor the low-level storm-track axis, a midlatitude oceanic frontal zone enhances the low-frequency variability of the midlatitude storm track and associated transport of heat and momentum by enhancing baroclinic eddy growth, which also acts to modify the variability of westerly jet streams. The presence of such a SST frontal zone as the APFZ can exert significant influence on the strength and structure of annular variability especially in winter, which is addressed in the next section.

4. Annular Modes simulated in the aqua-planet experiments

a. Identification of the Annular Modes

In order to identify the leading mode of low-frequency zonally symmetric variability in the model extratropical atmosphere, we applied an empirical orthogonal function (EOF)

analysis to the low-pass-filtered $[U_{250}]$ anomalies sampled every two days for 1800 days, separately for the individual hemispheres poleward of the latitude of 20° . In this EOF analysis, the anomaly fields were weighted by the square root of the Gaussian weight for a model grid, in consideration of latitudinal variations of the area each grid point represents. In good agreement with the previous studies (e.g., Thompson and Wallace 2000), the first EOF (EOF1) of $[U_{250}]$ anomalies represents “annular” variability for each of our experiments. Instead of displaying the obtained EOFs, we regressed the low-pass-filtered anomaly fields on the normalized leading principal component (PC1) time series for a particular hemisphere to depict typical anomalies associated with the “annular mode”. The regression maps represent the anomalies that would be observed when the PC1 time series increases by a unit standard deviation. Positive values of the PC1 time series correspond to the positive phase of the annular mode, or its “high-index” phase, characterized by the enhanced westerlies in higher latitudes. Typical anomalies for the negative phase, or the “low-index” phase, can be obtained by reversing the sign of the regressed anomalies.

Figure 6 shows the horizontal structure of the “annular mode” in our model experiments as the regressed local U anomalies at the 250-hPa and 925-hPa levels (U_{250} and U_{925} , respectively) for each of the model hemispheres. The model “annular mode” is characterized by a north-south seesaw in U between mid- and high latitudes. These U anomalies exhibit a high degree of zonal symmetry, especially in the CTL experiment, where the zonal symmetry is comparable with or even more pronounced than observed (e.g., Limpasuvan and Hartmann 2000), attributable to the zonally uniform lower-boundary conditions in our model experiments.

The dominance of these modes in low-frequency variability in the extratropical circulation can be seen in the fraction of the total $[U_{250}]$ variance explained by the PC1 (Table 1). In the summer hemisphere, the first mode explains nearly half of the total variance, about three times (twice) as much as the second mode does in the CTL (NF) experiment. These

features are in good agreement with those of the SAM in observations or in the previous GCM studies (e.g., Thompson and Wallace 2000; Hartmann and Lo 1998; Limpasuvan and Hartmann 2000). We therefore regard the particular EOF1 thus obtained as the counterpart of the SAM simulated in our idealized experiments. Note that the model NH corresponds to the summertime SH in observations but not to the NH. In the model winter hemisphere, the dominance of EOF1 in $[U_{250}]$ variability is reduced. Still, in the CTL experiment, the fraction of the total $[U_{250}]$ variance explained by EOF1 is significantly higher than that by the second EOF. In the NF experiment, however, the two leading EOFs account for comparable fractions of the total variance. Though rather annular, the structure of EOF1 in the NF experiment differs from that in the CTL experiment and the observed SAM, as shown later.

As the model EOF1 represents the dominant variability in $[U]$, the correlations between $[U_{250}]$ and the corresponding PC1 are markedly high around its centers of action, especially in the CTL experiment (Table 1). However, the correlation between local U (at individual longitudes) and the PC1 is less pronounced, in the presence of low-frequency zonally asymmetric variability (Fig. 6 and Table 1). The right column of Table 1 represents the zonal means of the local correlation between U and PC1 at the latitudes of the centers of action of the leading mode of $[U_{250}]$ variability. In fact, the particular correlation for the NF experiment is only 0.24~0.30 in strength even at the centers of action. Still, the corresponding correlation for the CTL experiment is stronger by about 0.15, except for the negative anomaly center in the winter hemisphere, which is located close to the intense STJ. These statistics suggest the augmented dominance of the annular mode in westerly wind variability in the presence of the frontal SST gradient in midlatitudes.

b. Structure of the annular modes

Figure 7 shows typical anomalies in zonal-mean zonal winds ($[U_{250}]$ and $[U_{925}]$) associated with the model annular mode. A meridional dipole in anomalous $[U]$ is evident in

each of the hemispheres (Fig. 7). In the CTL experiment, the node of the dipole is located at midlatitudes and the model annular mode represents north-south shifts of the PFJ axis, except in the wintertime upper troposphere, where the PFJ is not well separated from the STJ in the climatological mean state (Fig. 3; cf. Sampe et al. 2010). In the summer hemisphere of the CTL experiment (Fig. 7a), the positive and negative peaks in the $[U_{250}]$ anomalies are located at latitudes of 60° and 43° , respectively. These two centers of action with the node in between are reflected in the two midlatitude maxima of the variance of $[U_{250}]$ with the minimum in between (Fig. 4a), indicating the dominance of the annular mode in the $[U_{250}]$ variability. This node of the $[U_{250}]$ anomalies coincides with the joint axes of the time-mean PFJ and storm track. The $[U]$ anomalies exhibit nearly equivalent barotropic structure, although the center of negative $[U_{925}]$ anomalies is shifted slightly equatorward relative to its 250-hPa counterpart (Fig. 7c). The $[U_{925}]$ anomalies at the centers of action exhibit their correlation with the annular mode index (i.e., PC1) that is nearly as high as its counterpart for $[U_{250}]$, although the regressed anomalies are nearly half in amplitude (Figs. 6 and 7). The node of the $[U_{925}]$ anomalies is located at latitude of 50° , coinciding with the climatological axis of $[U_{925}]$ (Fig. 3b).

Figure 8 shows meridional profiles of $[U]$ composited separately for strong events of the positive and negative phases of the model annular modes (Fig. 8). The profiles again confirm that the model annular mode in the summer hemisphere for the CTL experiment represents north-south shifts of the PFJ axis (Fig. 8a and 8c). These profiles and the meridional structure of the $[U]$ anomalies described above overall resemble those of the observed summertime SAM, except for a slight poleward shift of the negative anomaly center in our model (Hartmann and Lo 1998; Thompson and Wallace 2000).

In the NF experiment, the amplitude and latitudinal structure of the $[U]$ anomalies over the summer hemisphere obviously differ from those in the CTL experiment (Figs. 6 and 7). Consistent with weakened $[U_{250}]$ fluctuations in the NF experiment (Fig. 4a), the strongest

anomaly associated with the annular mode is only $\sim 2.5 \text{ m s}^{-1}$ in $[U_{250}]$ and $\sim 1.5 \text{ m s}^{-1}$ in $[U_{925}]$. This amplitude of the annular variability is only about half of that in the CTL experiment (Fig. 7). It is also weaker than the maximum amplitude of the corresponding monthly anomalies associated with the observed SAM (Thompson and Wallace 2000), despite the zonally uniform lower-boundary conditions in our model. Moreover, the $[U]$ anomalies are less annular than those in the CTL experiment (Fig. 6 and Table 1). The positive and negative $[U_{250}]$ anomalies peak at latitudes of 49° and 31° , respectively, $\sim 10^\circ$ equatorward of their counterpart in the CTL experiment. The corresponding equatorward shift is also evident in the $[U_{925}]$ anomaly centers, reflecting the equivalent barotropic structure of the model annular mode. This equatorward displacement of the anomaly centers is in good correspondence to the displacement of the climatological westerlies, essentially in the same manner as observed for the summer-autumn difference in the SAM structure (Codron 2005). In fact, the nodes in $[U_{250}]$ and $[U_{925}]$ anomalies in the NF experiment are located in the vicinities of their mean axes and the collocated mean storm-track axes (Fig. 3), supporting the notion that the annular mode is a manifestation of north-south migrations of the PFJ (Fig. 8b). The displacement of the nodes of the annular mode is also consistent with the similar changes in the maxima of the $[U]$ variance (Fig. 4). Thus midlatitude frontal SST gradients exert significant impacts on the strength and meridional structure of the annular mode, the latter of which is found to change in conjunction with the displacement in the climatological joint axes of the PFJ and storm track.

A more significant impact of the SST front on the annular mode is evident in the winter hemisphere. In the CTL experiment, positive and negative $[U_{250}]$ anomalies associated with the positive phase of the annular mode peak at latitudes of 57° and 37° , respectively, with their node at 46° (Fig. 7b). Though weaker, a similar anomaly pattern is simulated in $[U_{925}]$ (Fig. 7d), indicating the equivalent barotropic structure of the annular mode. Compared to the upper-level anomalies, the subtropical center of action is less apparent in the $[U_{925}]$

anomalies. In the presence of the unrealistically strong STJ from which a PFJ is not well separated in the wintertime upper troposphere (Fig. 3a), the node of the $[U]$ anomaly does not correspond well to the mean westerly axis. Nevertheless, during strong positive events of the annular mode, a PFJ around 53° is separated unambiguously from the STJ in the upper troposphere (Fig. 8e). In the CTL experiment, enhanced eddy activity in the presence of the frontal SST gradient leads to rather frequent realizations of a PFJ-STJ double jet regime, as actually observed in the Southern Hemisphere (Aoki et al. 1996). The wintertime annular mode is manifested as transitions between this double-jet regime and the STJ-dominant single-jet regime in the upper troposphere, while it represents north-south migrations of the PFJ axis in the lower troposphere (Figs. 8e and 8g), as actually observed in winter over the Southeastern Indian Ocean in association with the SAM (Codron 2007). This feature in our experiment is in sharp contrast with that of the dominant annular variability in the presence of a strong STJ in an aqua-planet GCM experiment by Feldstein and Lee (1996), where the leading EOF represents a meridional displacement of the STJ. Rather, its counterpart in our CTL experiment represents a meridional seesaw in the midlatitude westerlies around the climatological storm-track axis (at $\sim 48^\circ$) with little changes in the STJ intensity.

In the NF experiment, the meridional structure of $[U]$ anomalies associated with the wintertime annular mode differs profoundly from that in the CTL experiment and in the observations. During positive events, positive $[U_{250}]$ anomalies prevail in midlatitudes. Their magnitude is, however, reduced by as much as 50% from the CTL experiment (Fig. 7b) and also considerably weaker than the amplitude of the SAM observed in monthly data (Thompson and Wallace 2000). The node of the $[U_{250}]$ anomalies is located at latitude of $\sim 32^\circ$ (Fig. 7b), with negative $[U_{250}]$ anomalies in the subtropics that are slightly stronger but more confined to the STJ axis. Thus, the anomaly pattern in $[U_{250}]$ appears to be distorted from the north-south dipole that characterizes its counterpart in the CTL experiment (Figs. 6 and 7). The weakening of the midlatitude anomalies seems to contribute to the reduction in the $[U_{250}]$

variance (Fig. 4a). No distinctive upper-level PFJ forms in midlatitudes even during strong positive events of the “annular mode” (Fig. 8f). Rather, this “annular mode” represents the weakening and strengthening of the STJ, as in one of the model experiments by Eichelberger and Hartmann (2007), in which a PFJ is not separated from an unrealistically intensified STJ. In the vertical structure, the midlatitude anomaly in the lower troposphere is nearly as strong as that in the upper troposphere, while the peak amplitude of the subtropical anomaly is reduced by ~60% from that in the upper troposphere (Fig. 7d). The lower-tropospheric annular variability represents changes in wind speed rather than the axial shifts of the westerlies (Fig. 8h).

One may notice that the climatological-mean $[U]$ in the NF experiment (Fig. 3) bears some resemblance to $[U]$ during extreme negative events of the annular mode in the CTL experiment (Fig. 8). In other words, the removal of the midlatitude frontal SST gradient acts to shift the mean circulation toward the situation corresponding to the negative phase of the annular mode realized in the presence of the SST front. The reduction in the midlatitude storm-track activity and associated poleward momentum transport, which acts to weaken a PFJ, is commonly seen in the mean state of the NF experiment and the negative phase of the annular mode (not shown). The resemblance between the annular mode anomalies and the NF-CTL differences in the mean state is consistent with the fact that annular modes can emerge either as atmospheric internal variability or as a response to axi-symmetric forcing in the extratropics (Ring and Plumb 2008).

In the winter hemisphere of the NF experiment, the fraction of $[U_{250}]$ variance explained by the EOF1 is comparable to that explained by the second or third EOF (Table 1) and thus smaller than in the CTL experiment and in the observations. We have examined the second and third EOFs for this hemisphere to see whether either of them represents annular variability similar to the observed SAM. Figure 9 shows meridional profiles of $[U_{250}]$ anomalies regressed linearly upon the PC time series for the three leading EOFs. None of

them resembles the anomaly pattern of the observed SAM. Thus, in the NF experiment, annular variability similar to the observed SAM cannot be reproduced in any of the (conventional) leading EOFs in the model winter hemisphere due to the lack of a frontal SST gradient.

c. Anomalies in transient eddy activity

Anomalies in the transient eddy forcing have been regarded as an important mechanism for maintaining $[U]$ anomalies associated with the annular modes (e.g., Karoly 1990). Figures 10 and 11 show meridional profiles of the regression coefficients of upper-level eddy amplitude, poleward eddy momentum flux and lower-tropospheric poleward eddy heat flux on the annular mode indices (PC1) in the summer and winter hemispheres, respectively, in our experiments. The poleward fluxes have been multiplied by the cosine of latitude in recognition of the dynamical importance of their meridional convergence. In the summer hemisphere of the CTL experiment, the upper-tropospheric eddy amplitude measured as the rms of 250-hPa eddy meridional wind velocity ($[v'_{250}]^{1/2}$) exhibits positive and negative anomaly centers at latitudes of $\sim 60^\circ$ and $\sim 42^\circ$, respectively, in the positive phase of the annular mode (Fig. 10a), representing a poleward displacement of the storm-track axis in conjunction with the corresponding shift of the PFJ axis (Fig. 7a). Anomalies in the upper-level poleward eddy transport of westerly momentum ($[u'v'_{250}]$) are strongest on the equatorward flank of the peak in the anomalous eddy amplitude (Fig. 10b), indicating anomalous equatorward wave-activity propagation. In general, transient eddies transport westerly momentum mainly from the subtropics into the vicinity of the midlatitude storm track (cf. Fig. 3d). Thus, the anomalous $[u'v'_{250}]$ with no significant negative values means that the westerly momentum transport is enhanced and extended poleward in association with the poleward migration of the storm-track axis during the positive events of the annular mode. The anomalous momentum transport converges and diverges around the peaks in the positive

and negative $[U]$ anomalies, respectively, to sustain them (Fig. 7a), which is consistent with the observed SAM.

The 850-hPa poleward eddy transport of sensible heat ($[v'T'_{850}]$) shows only weak anomalies with little correlation with the annular mode index over the entire hemisphere (Fig. 10c). The anomalies are stronger at the negative center of action ($\sim 45^\circ$) than at the positive center, presumably because of the larger mean eddy heat transport (Fig. 3e) due to intense surface baroclinicity associated with the frontal SST gradient. Lorenz and Hartmann (2001) argued that enhanced baroclinicity below the enhanced upper-level westerlies reinforces baroclinic eddy growth and the associated heat transport, leading to an increase in the convergence of eddy westerly momentum flux. Although this feedback may be operative weakly in this experiment, the eddy heat transport changes as little as $\sim 6\%$ of its time-mean value even at its negative anomaly center. Rather, much greater variability is found in $[u'v'_{250}]$, whose anomalies reach as much as 20~30% of its mean value (Fig. 10b). Therefore, the eddy forcing acting on the model annular mode is mostly barotropic forcing, whereas the eddy forcing of the observed SAM is both barotropic and baroclinic.

The elimination of the midlatitude frontal SST gradient leads to a weakening and equatorward shift in the anomalous eddy activity that accompanies the corresponding shift in the $[U]$ anomalies (Fig. 10). In the summer hemisphere of the NF experiment, the positive phase of the annular mode accompanies the positive anomaly in the upper-level eddy amplitude that peaks around latitude of $\sim 44^\circ$, slightly equatorward of the $[U]$ anomaly maximum (Fig. 7a). However, no substantial negative $[v'_{250}{}^2]^{1/2}$ anomaly is seen in the subtropics (Fig. 10a). In other words, the annular mode in the NF experiment accompanies coherent changes in eddy activity in both the subtropics and midlatitudes but not any apparent shift of the storm-track axis. Reflecting the modulations in both amplitude and horizontal structure of transient eddies (cf. Yu and Hartmann 1993), anomalous $[u'v'_{250}]$ is strongest at $\sim 40^\circ$ latitude and its anomalous convergence and divergence act to maintain the $[U]$

anomalies (Figs. 10b and 7a), as in the CTL experiment. Those anomalies in the upper-level eddy activity and momentum flux are, however, $\sim 40\%$ weaker than in the CTL experiment, consistent with the weaker $[U]$ anomalies. Fluctuations in the lower-tropospheric eddy heat transport ($[v'T'_{850}]$) associated with the annular mode are also weak, reflecting its very small climatological mean. In both of our experiments, the variance maxima of the eddy momentum transport (Fig. 4d) coincide with the peaks of its anomalies associated with the annular mode.

In the winter hemisphere of the CTL experiment, upper-level eddy amplitude measured as $[v'_{250}{}^2]^{1/2}$ increases in midlatitudes in association with the poleward shift of the storm-track axis during positive events of the annular mode (Fig. 11a). The upper-level poleward eddy momentum transport ($[-u'v'_{250}]$; i.e., southward transport in the SH) exhibits large positive anomalies around the node of the associated $[U]$ anomalies (Fig. 11b). This indicates enhanced equatorward wave-activity propagation from the intensified and poleward-shifted storm track. The associated enhancement in the poleward transport of westerly momentum acts to maintain the $[U]$ anomalies (Fig. 7b), as actually observed in association with the SAM (Hartmann and Lo 1998; Lorenz and Hartmann 2001). Stronger correlation of the annular mode index with the momentum transport compared to that with the eddy intensity confirms the importance of the barotropic eddy-mean flow interactions through modulations in horizontal structure of the eddies in the dynamics of the model annular mode. The peak of the eddy momentum transport anomaly again coincides with the peak of its low-frequency variance (Fig. 4d). Anomalies in the lower-tropospheric poleward eddy heat transport ($[-v'T'_{850}]$) peak around 55° , but both their amplitude and correlation with PC1 are quite weak (Fig. 11c).

In the NF experiment, anomalies in the upper-level eddy amplitude $[v'_{250}{}^2]^{1/2}$ are positive in a broad latitudinal range in the subtropics and midlatitudes during positive events of the annular mode, indicating an enhancement in eddy activity along the storm track (Fig. 11a). Unlike the observed SAM, there is no straightforward relationship between the

anomalies in $[U]$ and eddy intensity (Figs. 7b and 11a). Rather, the weakening of the STJ during positive events is accompanied by the enhancement of local eddy activity (Fig. 11a) in spite of the reduced vertical shear of $[U]$ (Figs. 7b and 7d). Though seemingly opposing to linear theories of baroclinic instability, this tendency is consistent with the fact that a strong STJ does not favor baroclinic eddy growth, as actually observed in the wintertime South Pacific and Indian Ocean (Nakamura and Shimpo 2004). Our result suggests that near-surface baroclinicity may be more important for baroclinic eddy growth than the baroclinicity in the free atmosphere that reflects the STJ intensity (Nakamura et al. 2004, 2008; Inatsu and Hoskins 2004; Sampe et al. 2010). The anomalous eddy momentum transport is convergent around 45° latitude, thereby acting to reinforce the positive $[U]$ anomaly (Fig. 11b). However, the anomalous eddy momentum transport is almost non-divergent in the subtropics, yielding no substantial contribution to the maintenance of the STJ anomaly that is nevertheless stronger than in the CTL experiment. The elimination of the midlatitude frontal SST gradient thus modulates the anomalous eddy activity associated with the annular mode into an unrealistic distribution with less robust signal of eddy-mean flow interaction. Lower-tropospheric eddy heat transport anomalies are positive around 48° latitude under the positive $[U_{250}]$ anomaly, while its peak does not coincide with the peak of the anomalous upper-level eddy intensity (Fig. 11c).

d. Characteristics of PC1 time series

Figure 12 shows the normalized PC1 time series for $[U_{250}]$ variability, or the “annular mode indices”, for the individual hemispheres in the CTL and NF experiments. Persistence and “redness” of the indices appear to differ among the four cases as indicated. Figure 13 shows the autocorrelation coefficients of the annular mode indices and Fig. 14 the power spectra of the indices. The autocorrelation reduces almost monotonously with lag until it approaches zero in all the cases. There is no indication of any dominant period of fluctuations

in either the autocorrelation (Fig. 13) or power spectra (Fig. 14). The annular mode index for the summer hemisphere of the CTL experiment shows marked persistence with e -folding lag of ~ 25 days (Fig. 13a), and its power spectrum exhibits pronounced “redness” (Fig. 14a). In the NF experiment, the power spectrum loses its “redness” substantially with e -folding lag of the autocorrelation reduced to ~ 10 days. In the model summer hemisphere, the elimination of the midlatitude frontal SST gradient thus acts to substantially reduce the persistence of the annular mode and its associated low-frequency variability. In the winter hemisphere, “redness” of the power spectra of the annular mode index is less than in the summer hemisphere (Fig. 14). The e -folding time of the autocorrelation is as small as ~ 10 days even in the CTL experiment (Fig. 13b). Nevertheless, the elimination of the frontal SST gradient leads to the reduction of persistence of the annular mode index also in the winter hemisphere, with the e -folding lag of ~ 6 days. This $\sim 60\%$ ($\sim 30\%$) reduction in the persistence of the annular mode for the summer (winter) hemisphere of the NF experiment may be due to weaker barotropic eddy forcing (Figs. 10b and 11b) and its positive feedback that acts to maintain the $[U]$ anomalies (cf. Lorenz and Hartmann 2001; Codron 2005).

Power spectra of the annular mode indices in observations and realistic model simulations have been shown to be statistically indistinguishable from the corresponding red-noise spectra (Hartmann and Lo 1998; Limpasuvan and Hartmann 2000). Figure 14 indicates, however, that the power spectra of the model annular modes tend to be different from the corresponding red-noise spectra, except for the summer hemisphere of the CTL experiment. Dynamics of the model annular mode appear to be distorted substantially by the elimination of the frontal SST gradient and also by the presence of a strong STJ in the winter hemisphere.

5. Summary and discussion

In the present study we have shown through aqua-planet AGCM experiments that the

influence of the midlatitude SST frontal zones is reflected in the annular variability of the extratropical troposphere. We have compared the simulated annular variability in the westerlies and associated storm-track modulations between the experiments with and without midlatitude frontal SST gradients as observed in the South Indian Ocean and assigned as the lower-boundary condition of our AGCM.

In the model summer hemisphere, the elimination of the midlatitude frontal SST gradient leads to a substantial weakening and equatorward shift of the variance maxima in both $[U]$ and poleward eddy transport of westerly momentum (Fig. 4), in correspondence to the shift of the joint axes of the climatological-mean PFJ and storm track (Fig. 3). In the winter hemisphere, the elimination of the frontal SST gradient yields a notable reduction in the $[U]$ variance along with a similar reduction in the variance of eddy momentum transport. The corresponding reduction is even greater in the variance of low-level poleward heat transport by transient eddies in both the winter and summer hemispheres (Fig. 4).

In order to depict systematic changes in the annular variability, we defined the first EOF of low-frequency $[U_{250}]$ anomalies as the “annular mode” in our model. In the summer hemisphere of the CTL experiment, the annular mode is manifested as north-south migrations of the PFJ (Fig. 8) and storm track, which yield anomalous eddy westerly momentum transport to sustain the $[U]$ anomalies (Fig. 10). Overall, the structures of the annular mode and associated eddy activity anomalies display no essential differences from their observational counterpart associated with the SAM, although the anomalies are somewhat displaced meridionally as a whole, corresponding to the displacement of the climatological-mean PFJ and storm track (Figs. 3, 7 and 10). In the NF experiment, anomalies in both $[U]$ and eddy activity are much weaker and the storm track exhibits no substantial axial shifts in association with the annular mode (Figs. 7 and 10). Compared to the CTL experiment, climatological-mean transient eddy activity and eddy momentum transport are both weaker (Fig. 3), leading to the weaker barotropic eddy forcing and the resultant

reductions in the amplitude and persistence of $[U]$ anomalies associated with the annular mode (Fig. 13a).

In the winter hemisphere where the STJ intensifies, north-south shifts of the PFJ are evident only in the lower troposphere. In the CTL experiment, the amplitude of the annular mode is as large as that in the summer hemisphere, and a PFJ is well separated from the STJ during strong positive events of the annular mode (Fig. 8). The climatologically strong eddy activity can impose strong barotropic forcing on $[U]$ anomalies, as in the observed SAM (Fig. 11). In the NF experiment, the amplitude of midlatitude $[U]$ anomalies associated with the “annular mode” is about a half of that in the CTL experiment (Fig. 7), and the anomalous divergence of eddy momentum transport does not contribute substantially to the maintenance of subtropical $[U]$ anomalies (Fig. 11). In the absence of the midlatitude frontal SST gradient, the STJ is intense and eddy activity is climatologically suppressed, which is not favorable for yielding positive feedback to prolong the persistence of the $[U]$ anomalies (Eichelberger and Hartmann 2007; Lorenz and Hartmann 2001).

Though idealized, our model experiments suggest the significance of midlatitude oceanic frontal zones for the atmosphere in yielding annular variability with realistic strength, latitudinal structure and associated eddy-mean flow interactions. The elimination of the midlatitude frontal SST gradient weakens the midlatitude storm-track activity and the eddy-driven PFJ, thus diminishing the annular variability of $[U]$ that is driven mainly through the positive eddy- $[U]$ feedback associated with a meridionally migrating storm track. Therefore, the impacts of midlatitude frontal SST gradients are not limited to the mean state of the extratropical tropospheric circulation (Sampe et al. 2010) but extend onto its dominant variability via modulations of transient eddy activity, as demonstrated in the present study.

One should keep it in mind that the primary purpose of the present study is to assess potential impacts of the midlatitude frontal SST gradient on annular variability of the extratropical atmosphere, but not to reproduce their observational counterpart in the SH. The

impact must be overestimated to some extent in our experiments if compared with the observed SH situation. One of the factors for the overestimation is the minimum SST that is set to be 0 °C, which keeps the equator-pole surface temperature difference smaller than that in the real atmosphere. Nevertheless, the surface baroclinicity in polar regions may not profoundly affect a midlatitude storm track and PFJ in our simulation, since the primary storm track over the South Indian Ocean is observed in midlatitudes, away from the strong surface baroclinic zone along the sea-ice edge off Antarctica (Nakamura and Shimpo 2004). Another factor for the overestimation is the zonally uniform SST prescribed in our experiments. In reality, the SST gradient and the axial latitude of oceanic frontal zones exhibits a certain degree of zonal asymmetry. In fact, the SST gradient along APFZ is strongest in the western portion of the South Indian Ocean (Nakamura and Shimpo 2004; Inatsu and Hoskins 2004), and the meridional SST profile in this longitudinal sector is prescribed at every longitude in our CTL experiment. It is therefore likely that the impact of the frontal SST gradient on the annular variability of the extratropical atmosphere simulated in the present study is overestimated and should therefore be regarded as an upper bound of its potential impact.

Our model experiments nevertheless suggest at least two factors that are necessary for reproducing annular modes in AGCM simulations with realistic amplitude and structure. First, transient eddy activity in midlatitudes should be strong enough to maintain a well-defined PFJ and exert barotropic forcing for driving its axial migrations. In our aqua-planet setting, the presence of the midlatitude SST frontal zone sustains intense storm-track activity in midlatitudes through maintaining strong near-surface baroclinicity (Sampe et al. 2010). Lorenz and Hartmann (2001) argued that external diabatic forcing, including SST gradient, with meridionally uniform profile is favorable for persistence of the anomalies of a westerly jet and synoptic-scale eddies, because they could stay embedded in constant external forcing even if they migrate meridionally from their climatological position. In the summer hemisphere of our experiments, however, the annular mode in the absence of

the frontal SST gradient tends to be less persistent. While acting to anchor a storm track (Fig. 5), the frontal SST gradient augments both mean eddy activity and its variability and thereby enhances annular variability of the extratropical atmosphere.

Second, the STJ should not be excessively strong to retain the structure of the annular mode as observed, which tends to be distorted in the presence of the strong STJ. Negative impacts that can be exerted by a strong STJ on the amplitude and structure of annular modes have also been suggested by Eichelberger and Hartmann (2007). Numerical experiments, including our NF experiment, suggest that a predominant STJ with no well-defined PFJ can render the annular variability essentially different from the observed SAM. In fact, the dominant annular variability represents a north-south migration of a STJ in an aqua-planet experiment by Feldstein and Lee (1996), in which the simulated STJ is strong and no frontal temperature gradient is prescribed at the surface. The importance of oceanic frontal zones suggested by our experiments may have some implications for the issue to what extent the annular variability in idealized numerical experiments can be used for discussing the annular mode in the real atmosphere.

In a framework postulated by Nakamura et al. (2004), the atmospheric general circulation in the extratropics can be better understood as a coupled system of the interacting atmosphere and ocean, with a link among a midlatitude oceanic frontal zone, storm track and PFJ. The results of the present study suggest that this framework is also effective in understanding the observed annular variability in the extratropical atmosphere. Nakamura et al. (2004) also argued the possibility of a feedback loop among a midlatitude oceanic frontal zone, storm track and the surface westerlies through the maintenance of atmospheric surface baroclinicity (Nonaka et al. 2009; Taguchi et al. 2009; Sampe et al. 2010; Hotta and Nakamura 2011), westerly momentum transport and surface wind stress that drives ocean circulation. Recently, variations in ocean circulation, SST and sea ice extent associated with the SAM have been explored (e.g., Sen Gupta and England 2006; Ciasto and Thompson 2008).

Hall and Visbeck (2002) found that a more intense circumpolar current is closely associated with the positive phase of the SAM in their coupled ocean-atmosphere GCM experiment, suggesting that the SAM is a source of large-scale variability in the SH ocean. How such oceanic variability as above can exert feedback to the atmosphere and whether this feedback, if any, is significant in the presence of vigorous atmospheric internal variability are open questions. The role of the atmosphere-ocean interactions in the SH annular mode will continue to be an intriguing issue on climate variability.

Acknowledgments

We used the Earth Simulator under the support of the Japan Agency for Marine-Earth Science and Technology (JAMSTEC). We appreciate helpful advice by the AFES/CFES working team at JAMSTEC. This study is supported through the Grant-in-Aids for Scientific Research #18204044, #22340135 and on Innovative Areas #2205 by the Japanese Ministry of Education, Culture, Sports, Science and Technology (MEXT) and also through the Global Environment Research Fund (S-5) by the Japanese Ministry of Environment.

References

- Aoki, H., M. Shiotani, and I. Hirota, 1996: Interannual variability of the tropospheric circulation in relation to the stratosphere in the Southern Hemisphere. *J. Meteor. Soc. Japan*, **74**, 509–523.
- Brayshaw, D. J., B. J. Hoskins, and M. Blackburn, 2008: The storm-track response to idealized SST perturbations in an aquaplanet GCM. *J. Atmos. Sci.*, **65**, 2842–2860.
- Charney, J. G., 1947: The dynamics of long waves in a baroclinic westerly current. *J. Meteor.*, **4**, 135–162.
- Chen, G., R. A. Plumb, and J. Lu, 2010: Sensitivities of zonal mean atmospheric circulation to SST warming in an aqua-planet model. *Geophys. Res. Lett.*, **37**, L12701, doi:10.1029/2010GL043473.
- Ciasto, L. M., and D. W. J. Thompson, 2008: Observations of large-scale ocean-atmosphere interaction in the Southern Hemisphere. *J. Climate*, **21**, 1244–1259.
- Codron, F., 2005: Relation between annular modes and the mean state: Southern Hemisphere summer. *J. Climate*, **18**, 320–330.
- Codron, F., 2007: Relations between annular modes and the mean state: Southern Hemisphere winter. *J. Atmos. Sci.*, **64**, 3328–3339.
- DeWeaver, E., and S. Nigam, 2000: Do stationary waves drive the zonal-mean jet anomalies of the northern winter? *J. Climate*, **13**, 2160–2176.
- Eady, E. T., 1949: Long waves and cyclone waves. *Tellus*, **1**, 33–52.
- Eichelberger, S. J., and D. L. Hartmann, 2007: Zonal jet structure and the leading mode of variability. *J. Climate*, **20**, 5149–5163.
- Feldstein, S. B., and S. Lee, 1996: Mechanisms of zonal index variability in an aquaplanet GCM. *J. Atmos. Sci.*, **53**, 3541–3555.
- Hall, A., and M. Visbeck, 2002: Synchronous variability in the Southern Hemisphere atmosphere, sea ice, and ocean resulting from the annular mode. *J. Climate*, **15**,

3043-3057.

- Hartmann, D. L., and F. Lo, 1998: Wave-driven zonal flow vacillation in the Southern Hemisphere. *J. Atmos. Sci.*, **55**, 1303-1315.
- Hotta, D., and H. Nakamura, 2011: On the significance of sensible heat supply from the ocean in the maintenance of mean baroclinicity along storm tracks. *J. Climate*, **24**, in press.
- Inatsu, M., and B. J. Hoskins, 2004: The zonal asymmetry of the Southern Hemisphere winter storm-track. *J. Climate*, **17**, 4882-4891.
- Karoly, D. J., 1990: The role of transient eddies in the low-frequency zonal variations in the Southern Hemisphere circulation. *Tellus*, **42A**, 41-50.
- Kidson, J. W., 1988: Indices of the Southern Hemisphere zonal wind. *J. Climate*, **1**, 183-194.
- Kidson, J. W., and M. R. Sinclair, 1995: The influence of persistent anomalies on Southern Hemisphere storm tracks. *J. Climate*, **8**, 1938-1950.
- Kimoto, M., F.-F. Jin, M. Watanabe, and N. Yasutomi, 2001: Zonal-eddy coupling and a neutral mode theory for the Arctic Oscillation. *Geophys. Res. Lett.*, **28(4)**, 737-740.
- Limpasuvan, V., and D. L. Hartmann, 2000: Wave-maintained annular modes of climate variability. *J. Climate*, **13**, 4414-4429.
- Lorenz, E. N., 1951: Seasonal and irregular variations of the Northern Hemisphere sea-level pressure profile. *J. Meteor.*, **8**, 52-59.
- Lorenz, D. J., and D. L. Hartmann, 2001: Eddy-zonal flow feedback in the Southern Hemisphere. *J. Atmos. Sci.*, **58**, 3312-3327.
- Nakamura, H., and T. Sampe, 2002: Trapping of synoptic-scale disturbances into the North-Pacific subtropical jet core in midwinter. *Geophys. Res. Lett.*, **29**, doi:1029/2002GL015335.
- Nakamura, H., and A. Shimpo, 2004: Seasonal variations in the Southern Hemisphere storm tracks and jet streams as revealed in a reanalysis dataset. *J. Climate*, **17**, 1828-1844.
- Nakamura, H., T. Sampe, Y. Tanimoto, and A. Shimpo, 2004: Observed associations among

- storm tracks, jet streams and midlatitude oceanic fronts. *Earth's Climate: The Ocean-Atmosphere Interaction*, C. Wang, S.-P. Xie and J. A. Carton, Eds., Geophys. Monogr., American Geophysical Union, pp.329-345.
- Nakamura, H., T. Sampe, A. Goto, W. Ohfuchi, and S.-P. Xie, 2008: On the importance of midlatitude oceanic frontal zones for the mean state and dominant variability in the tropospheric circulation. *Geophys. Res. Lett.*, **35**, L15709, doi:10.1029/2008GL034010.
- Namias, J., 1950: The index cycle and its role in the general circulation. *J. Meteor.*, **7**, 130-139.
- Nonaka, M., H. Nakamura, B. Taguchi, N. Komori, A. Yoshida-Kuwano, and K. Takaya, 2009: Air-sea heat exchanges characteristic to a prominent midlatitude oceanic front in the South Indian Ocean as simulated in a high-resolution coupled GCM. *J. Climate*, **22**, 6515-6535.
- Ohfuchi, W., H. Nakamura, M. Yoshioka, T. Enomoto, K. Takaya, X. Peng, S. Yamane, T. Nishimura, Y. Kurihara, and K. Ninomiya, 2004: 10-km mesh meso-scale resolving global simulations of the atmosphere on the Earth Simulator — Preliminary outcomes of AFES (AGCM for the Earth Simulator). *J. Earth Simulator*, **1**, 8-34.
- Ohfuchi, W., H. Sasaki, Y. Masumoto, and H. Nakamura, 2007: “Virtual” atmospheric and oceanic circulation in the Earth Simulator. *Bull. Amer. Meteor. Soc.*, **88**, 861-866.
- Ring, M. J., and R. A. Plumb, 2008: The response of a simplified GCM to axisymmetric forcings: Applicability of the fluctuation-dissipation theorem. *J. Atmos. Sci.*, **65**, 3880-3898.
- Robinson, W. A., 1991: The dynamics of the zonal index in a simple model of the atmosphere. *Tellus*, **43A**, 295-305.
- Robinson, W. A., 2006: On the self-maintenance of midlatitude jets. *J. Atmos. Sci.*, **63**, 2109-2122.
- Rossby, C.-G., 1939: Relation between variations in the intensity of the zonal circulation of

- the atmosphere and the displacements of the semi-permanent centers of action. *J. Mar. Res.*, **2**, 38-55.
- Sampe, T., H. Nakamura, A. Goto, and W. Ohfuchi, 2010: Significance of a midlatitude SST frontal zone in the formation of a storm track and an eddy-driven westerly jet. *J. Climate*, **23**, 1793-1814.
- Sen Gupta, A., and M. H. England, 2006: Coupled ocean–atmosphere–ice response to variations in the Southern Annular Mode. *J. Climate*, **19**, 4457-4486.
- Shiogama, H., T. Terao, and H. Kida, 2004: The role of high-frequency eddy forcing in the maintenance and transition of the Southern Hemisphere annular mode. *J. Meteor. Soc. Japan*, **82**, 101-113.
- Stone, P. H., 1978: Baroclinic adjustment. *J. Atmos. Sci.*, **35**, 561-571.
- Taguchi, B., H. Nakamura, M. Nonaka, and S.-P. Xie, 2009: Influences of the Kuroshio/Oyashio Extensions on air-sea heat exchanges and storm track activity as revealed in regional atmospheric model simulations for the 2003/4 cold season. *J. Climate*, **22**, 6536-6560.
- Thompson, D. W. J., and J. M. Wallace, 1998: The Arctic Oscillation signature in the wintertime geopotential height and temperature fields. *Geophys. Res. Lett.*, **25**, 1297-1300.
- Thompson, D. W. J., and J. M. Wallace, 2000: Annular modes in the extratropical circulation. Part I: Month-to-month variability. *J. Climate*, **13**, 1000-1016.
- Yoden, S., M. Shiotani, and I. Hirota, 1987: Multiple planetary flow regimes in the Southern Hemisphere. *J. Meteor. Soc. Japan*, **65**, 571-586.
- Yu, J.-Y., and D. L. Hartmann, 1993: Zonal flow vacillation and eddy forcing in a simple GCM of the atmosphere. *J. Atmos. Sci.*, **50**, 3244-3259.

Tables and Figures

		$[U_{250}]$ explained variance	$[U_{250}]$ -PC1 correlation	U_{250} -PC1 correlation averaged zonally
		mode 1 (2, 3)	positive/negative	positive/negative
CTL	summer	54 (18, 12)	0.93/-0.94	0.46/-0.37
NF	summer	40 (23, 11)	0.83/-0.70	0.29/-0.24
CTL	winter	37 (28, 17)	0.94/-0.80	0.41/-0.25
NF	winter	29 (24, 22)	0.83/-0.71	0.25/-0.30

Table 1. (left) Percentage of the total variance in 250-hPa zonal-mean zonal wind $[U_{250}]$ explained by the three leading EOFs based on low-pass-filtered fields from the 60-month model CTL and NF integrations. An EOF analysis was applied to each of the model summer and winter hemispheres in the region poleward of latitude of 20° . (middle) Correlation coefficients between $[U_{250}]$ and PC1 at their positive and negative anomaly centers, and (right) zonally averaged correlation coefficients between local U_{250} and PC1 at the latitudes of their positive and negative anomaly centers.

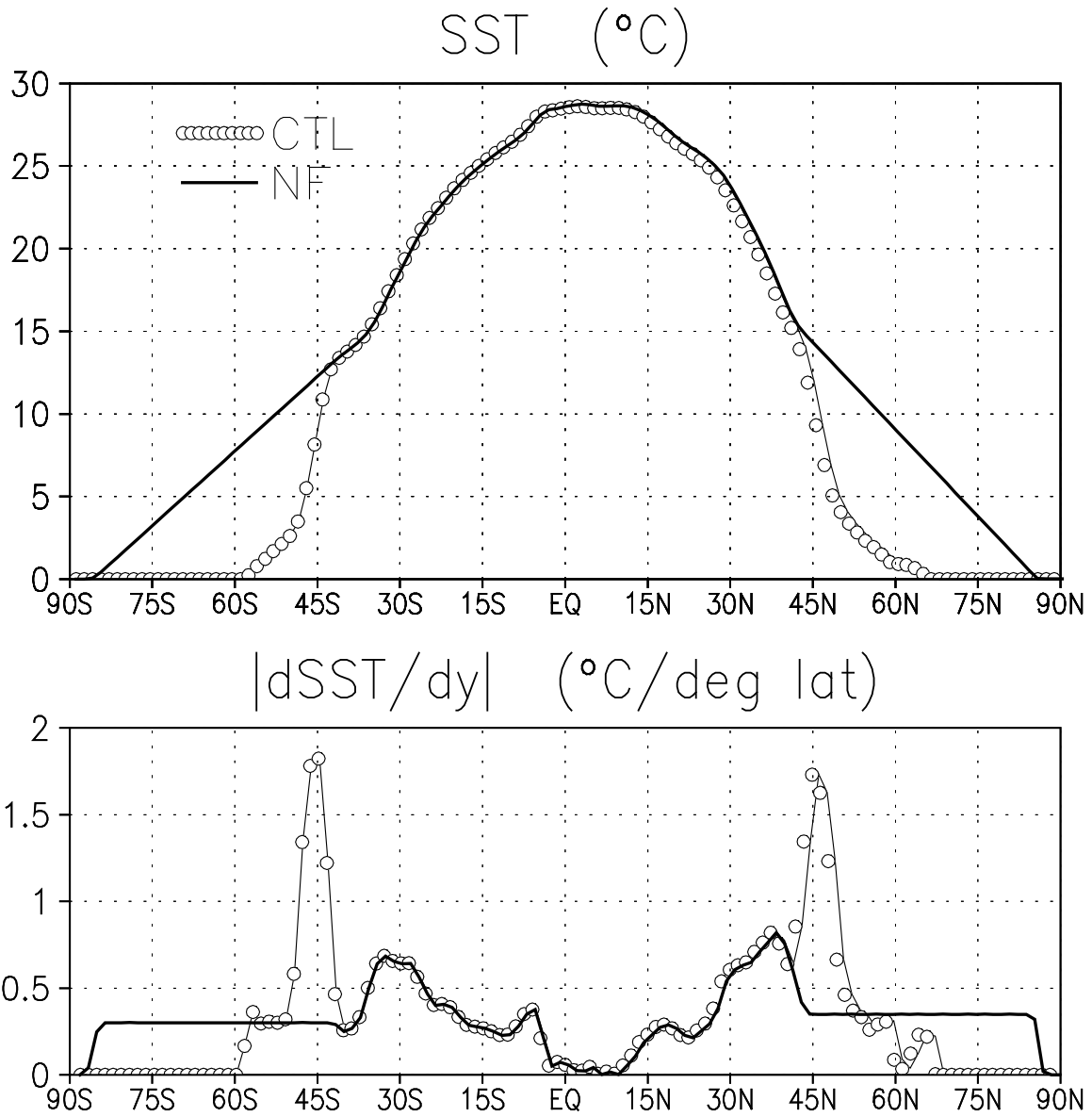


Fig. 1. SST profiles (upper panel; $^{\circ}\text{C}$) and magnitude of their meridional gradient (lower panel; $^{\circ}\text{C} (110 \text{ km})^{-1}$) prescribed as the lower-boundary condition of the model for CTL (thin line with open circles) and NF (thick line) experiments. Sharp midlatitude SST gradients in the CTL experiment are replaced with small, constant gradient of $0.3 \text{ }^{\circ}\text{C} (110 \text{ km})^{-1}$ for the SH and $0.35 \text{ }^{\circ}\text{C} (110 \text{ km})^{-1}$ for the NH in the NF experiment.

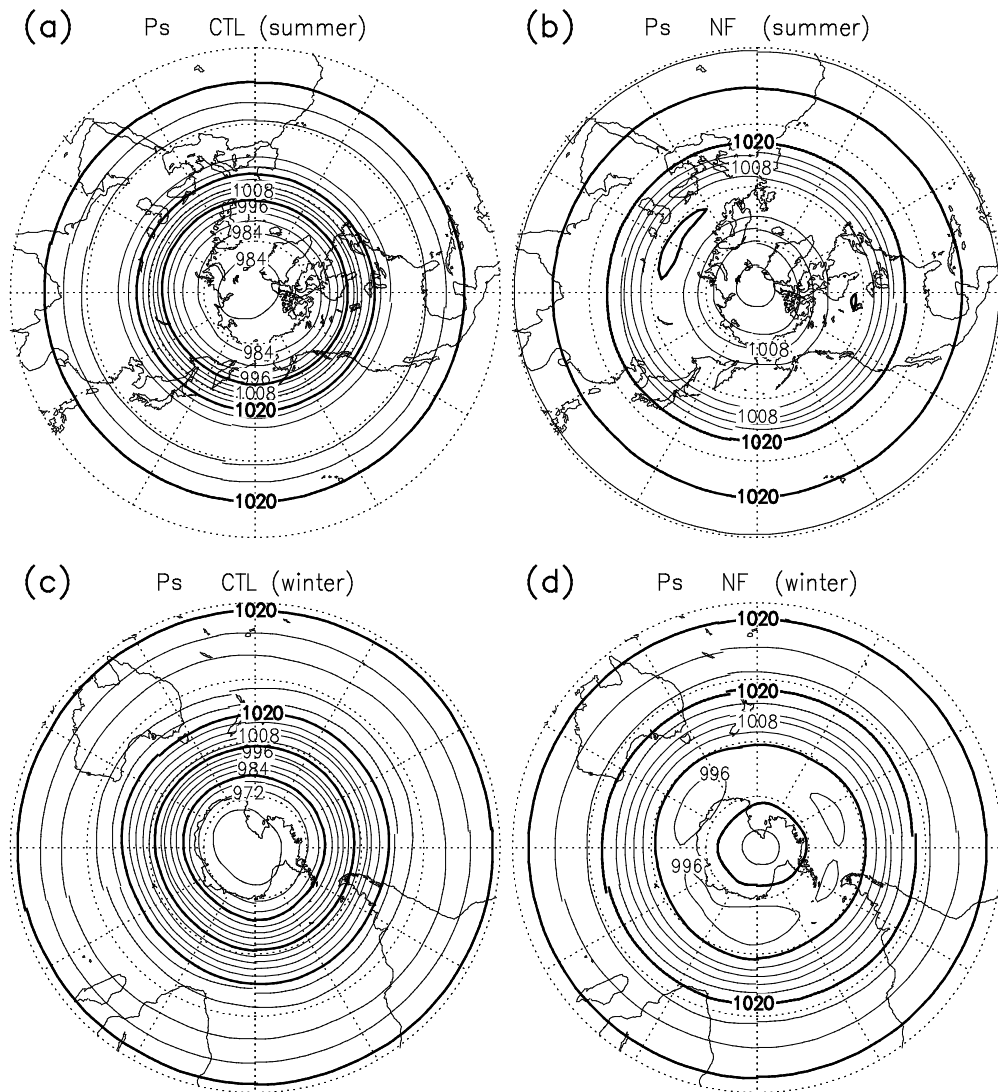


Fig. 2. Climatological-mean fields of sea-level pressure (hPa) for the 60-month model integration over the (a) summer hemisphere of the CTL experiment, (b) summer hemisphere in the NF experiment, (c) winter hemisphere of the CTL experiment and (d) winter hemisphere of the NF experiment. Contour intervals are 4 hPa for thin lines and 20 hPa for thick lines. Although no landmass is prescribed in our experiments, coastlines are drawn to help the readers identify latitudes.

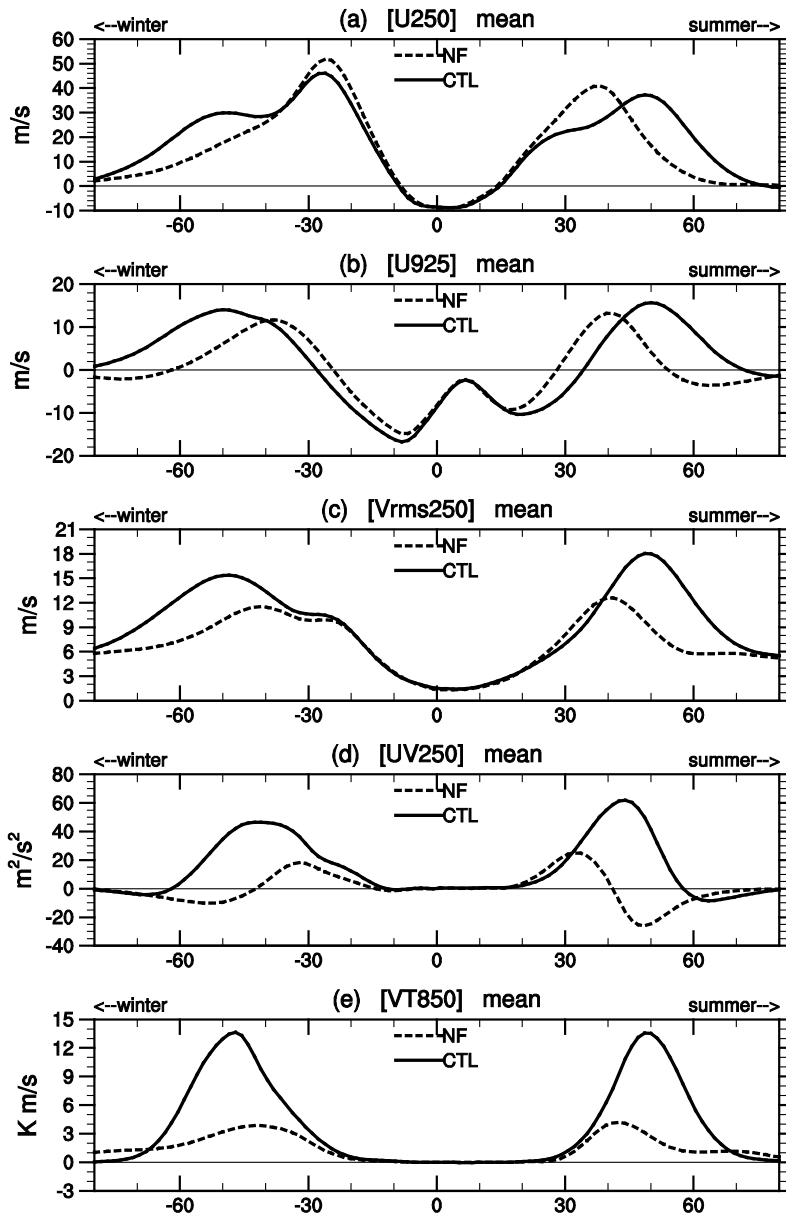


Fig. 3. (a-b) Meridional profiles for the climatological-mean zonal-mean zonal wind [U] (m s^{-1}) at the (a) 250-hPa and (b) 925-hPa levels. Solid line for the CTL experiment and dashed line for the NF experiment. The model NH (SH) corresponds to the summer (winter) hemisphere. (c) As in (a), but for rms of eddy meridional wind fluctuations (m s^{-1}) at the 250-hPa level ($[v'_{\text{rms } 250}]$). (d) As in (a), but for 250-hPa poleward eddy flux of westerly momentum ($\text{m}^2 \text{s}^{-2}$). (e) As in (a), but for poleward eddy transport of sensible heat (K m s^{-1}) at the 850-hPa level.

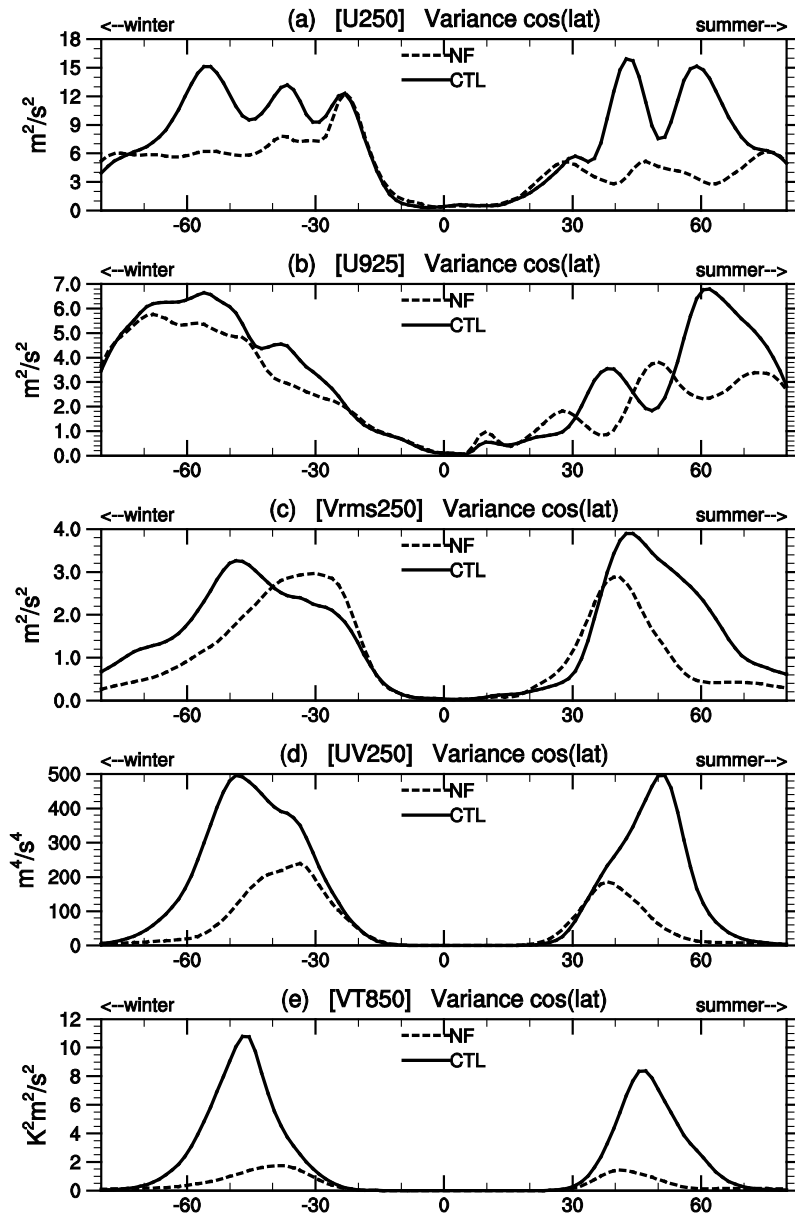


Fig. 4. (a) Meridional profile of the low-frequency variance of 250-hPa zonal-mean zonal wind $[U]$ ($m^2 s^{-2}$). Solid line is for the CTL experiment and dashed line for the NF experiment. (b) As in (a), but for the variance of 925-hPa $[U]$. (c) As in (a), but for the zonally averaged low-frequency variance of the amplitude (rms) of 250-hPa eddy meridional wind ($[v'^2_{250}]^{1/2}$; $m^2 s^{-2}$). (d) As in (c), but for the low-frequency variance of 250-hPa poleward eddy flux of westerly momentum ($[u'v'_{250}]$; $m^4 s^{-4}$). (e) As in (c), but for the low-frequency variance of 850-hPa poleward eddy flux of sensible heat ($[v'T'_{850}]$; $K^2 m^2 s^{-2}$). The cosine of latitude was multiplied to the variance to represent latitudinal dependence of the grid area.

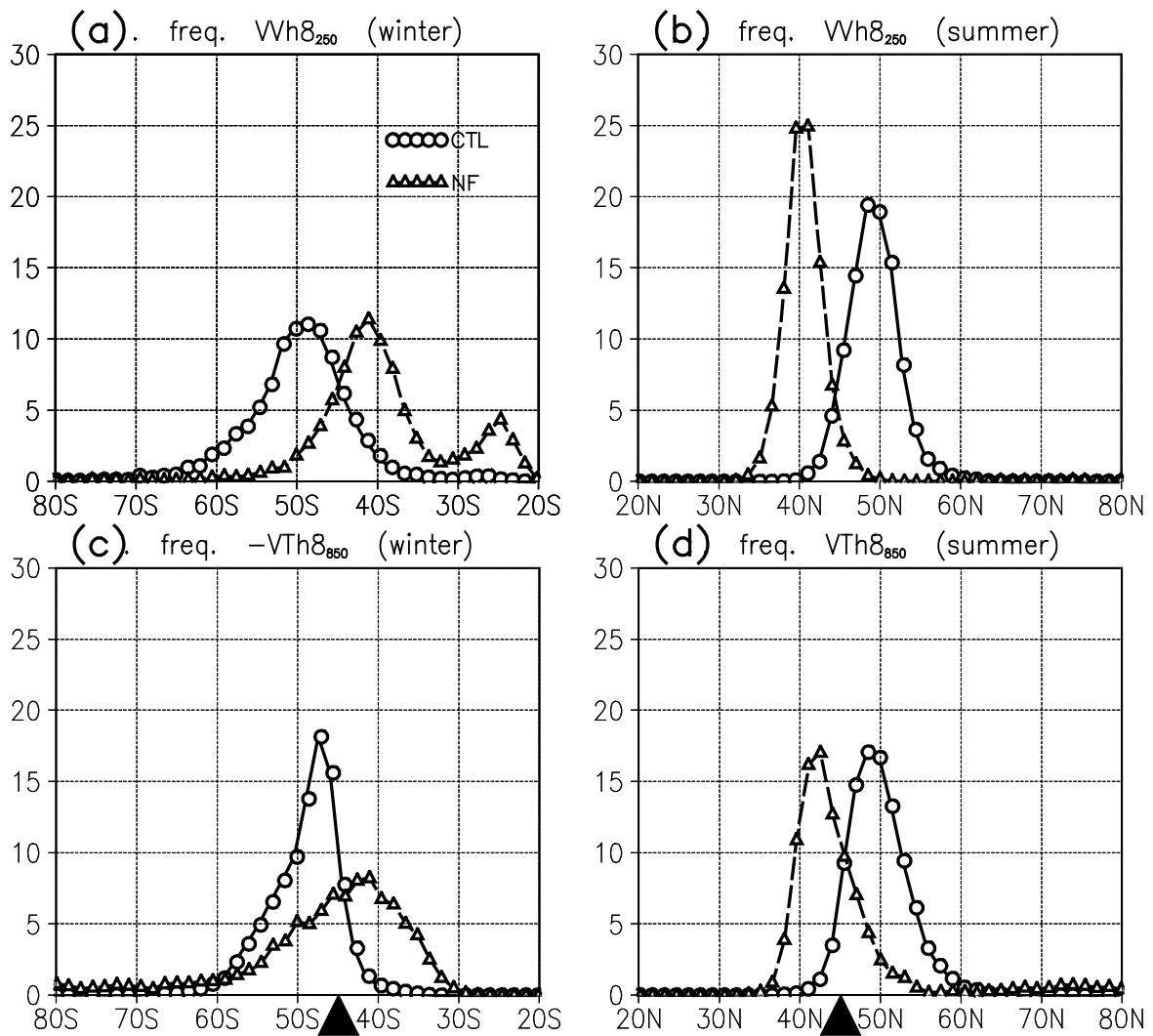


Fig. 5. Frequency distribution of the instantaneous axial latitude of the primary storm track represented as the percentage of the periods relative to the entire data length of 1800 days. (a, b) Based on the zonal-mean variance of 250-hPa eddy meridional wind velocity ($[v'^2_{250}]$) for the (a) winter and (b) summer hemispheres. (c, d) As in (a, b), respectively, but based on the zonal-mean 850-hPa poleward eddy heat flux ($[v'T'_{850}]$). Large black triangles indicate the latitudes of the SST fronts in the CTL experiment.

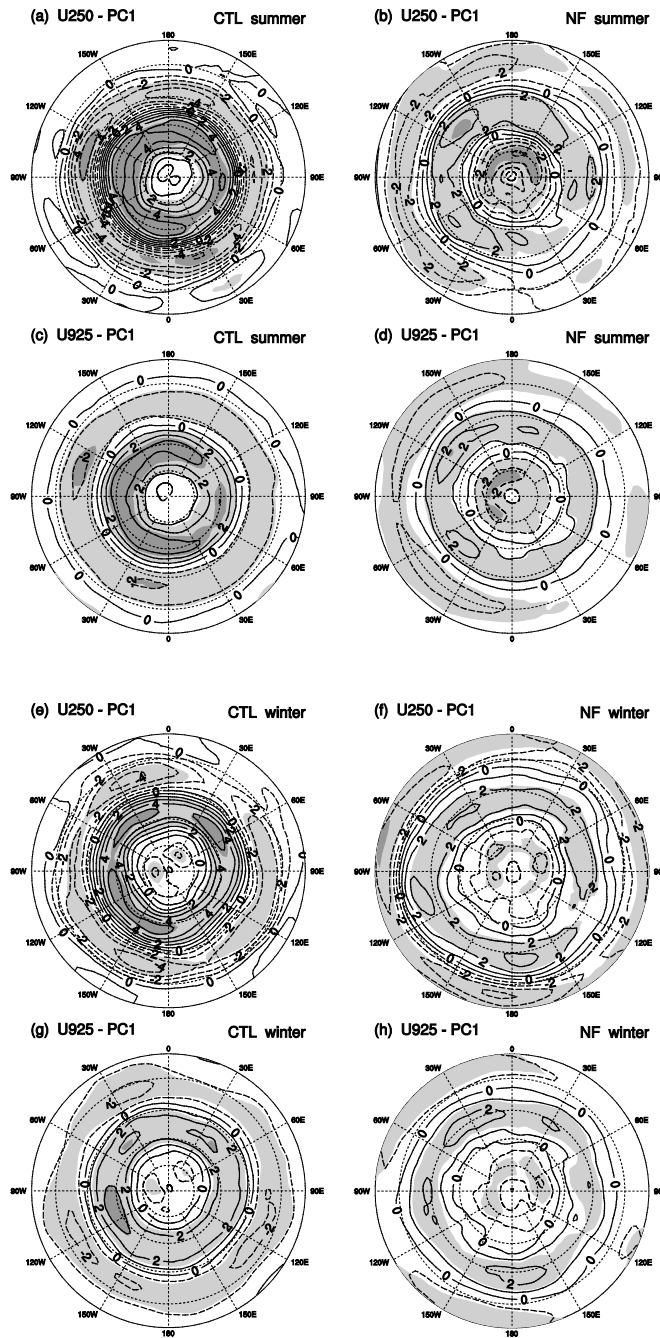


Fig. 6. Regression maps of zonal wind velocity U (m s^{-1}) on the “annular mode index” (PC1) for the CTL (left panels) and NF (right panels) experiments. (a-d) At the (a, b) 250-hPa and (c, d) 925-hPa levels in the summer hemisphere. (e-h) At the (e, f) 250-hPa and (g, h) 925-hPa levels in the winter hemisphere. Negative contours are dashed. Light and dark shadings indicate the magnitude of the local correlation coefficients is 0.2~0.4 and greater than 0.4, respectively. The correlation greater than 0.21 in magnitude is significant at the 95% confidence level. Poleward of the latitude of 20° is plotted.

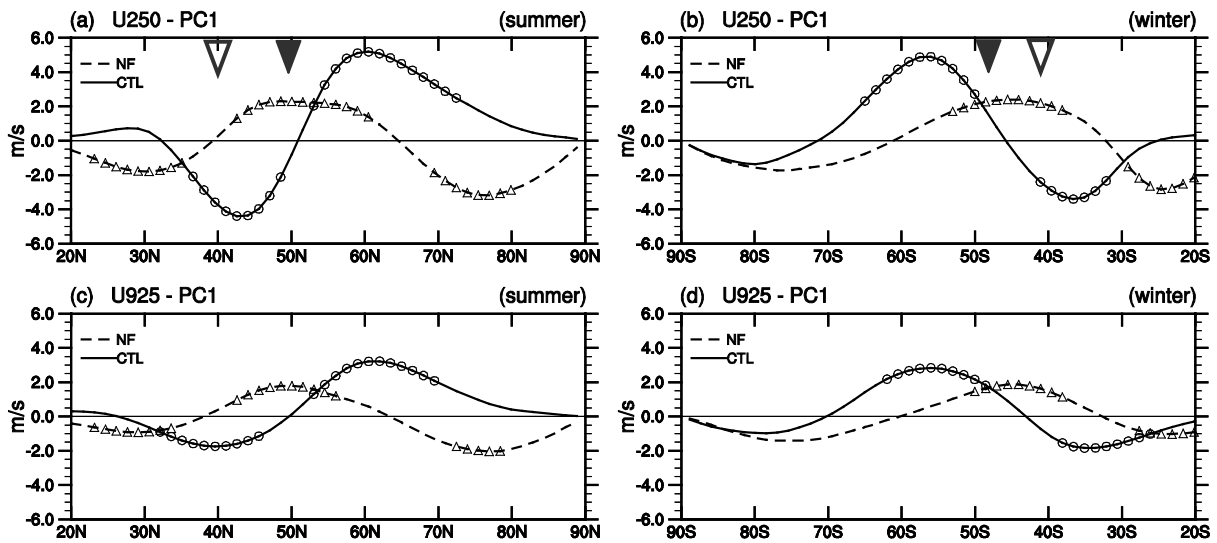


Fig. 7. Meridional profiles of regression coefficient of zonal-mean zonal wind [U] (m s^{-1}) at the (a, b) 250-hPa and (c, d) 925-hPa levels on the annular mode index for (a, c) the summer hemisphere and (b, d) the winter hemisphere. Solid lines are for the CTL experiment and dashed lines for the NF experiment, with circles and triangles indicating the corresponding correlation greater than 0.5 in magnitude. Filled and open triangles on the upper fringe of the upper panels indicate the latitudes of the climatological-mean 250-hPa storm track axes in the CTL and NF experiments, respectively.

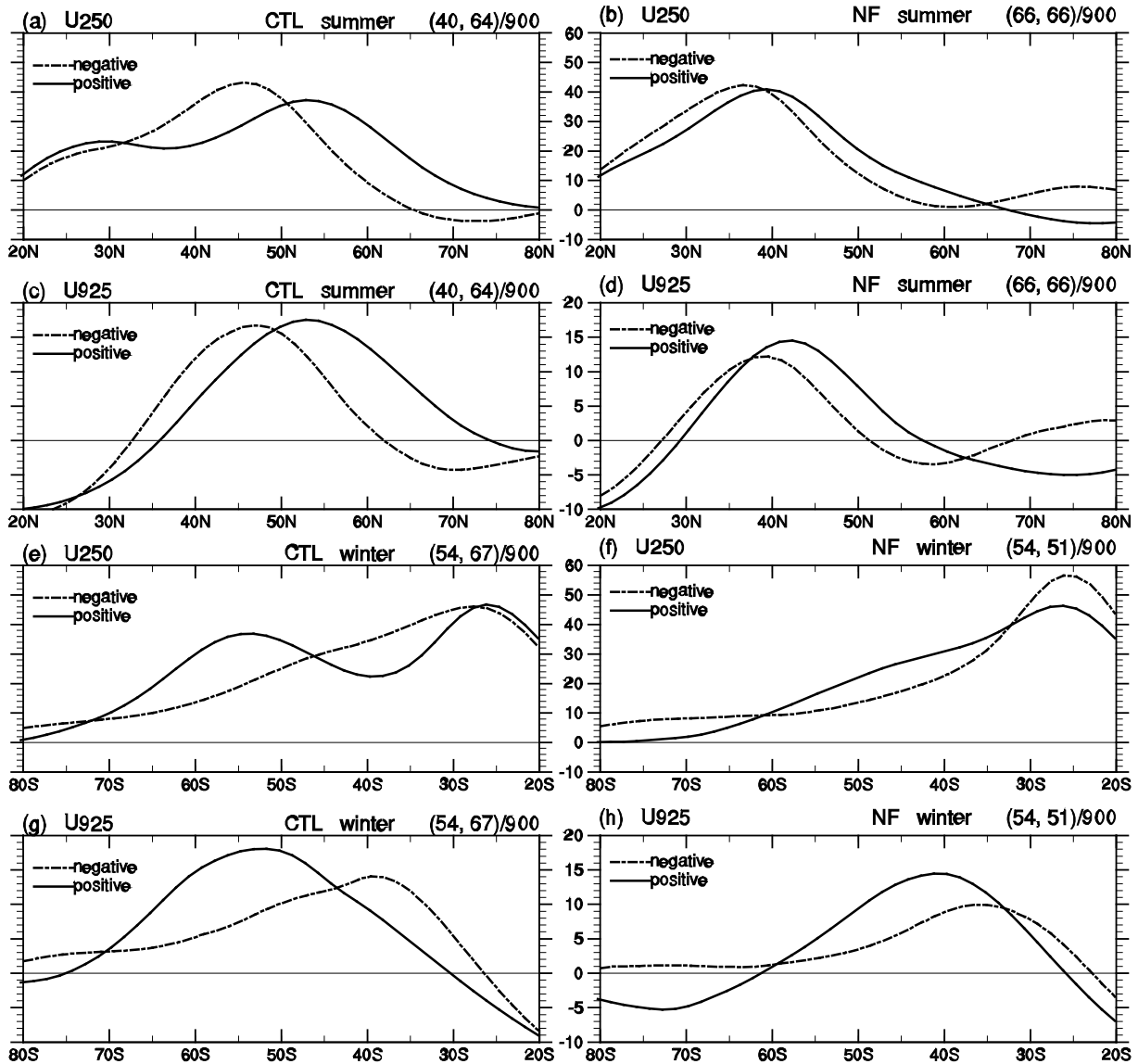


Fig. 8. Composite meridional profiles of zonal-mean zonal wind [U] (m s^{-1}) for periods with the annular mode index greater than $+1.5$ (positive events; solid line) and less than -1.5 (negative events; dot-dashed line) in the (left panels) CTL and (right panels) NF experiments. At the (a, b) 250-hPa and (c, d) 925-hPa levels for the summer hemisphere, and at the (e, f) 250-hPa and (g, h) 925-hPa levels for the winter hemisphere. The numbers of the composited days are shown in parenthesis (“positive”, “negative”) on the right hand side above each panel.

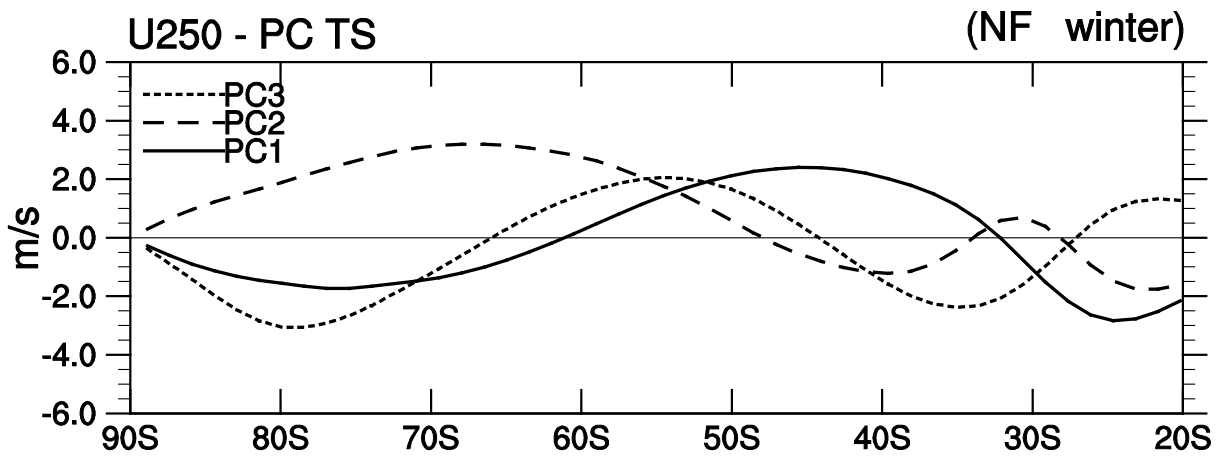


Fig. 9. Latitudinal profiles of the regression coefficients of 250-hPa zonal-mean zonal wind [U_{250}] (m s^{-1}) on the PC1 (annular mode index; solid line), PC2 (long dashed line) and PC3 (dotted line) time series for the winter hemisphere of the NF experiment.

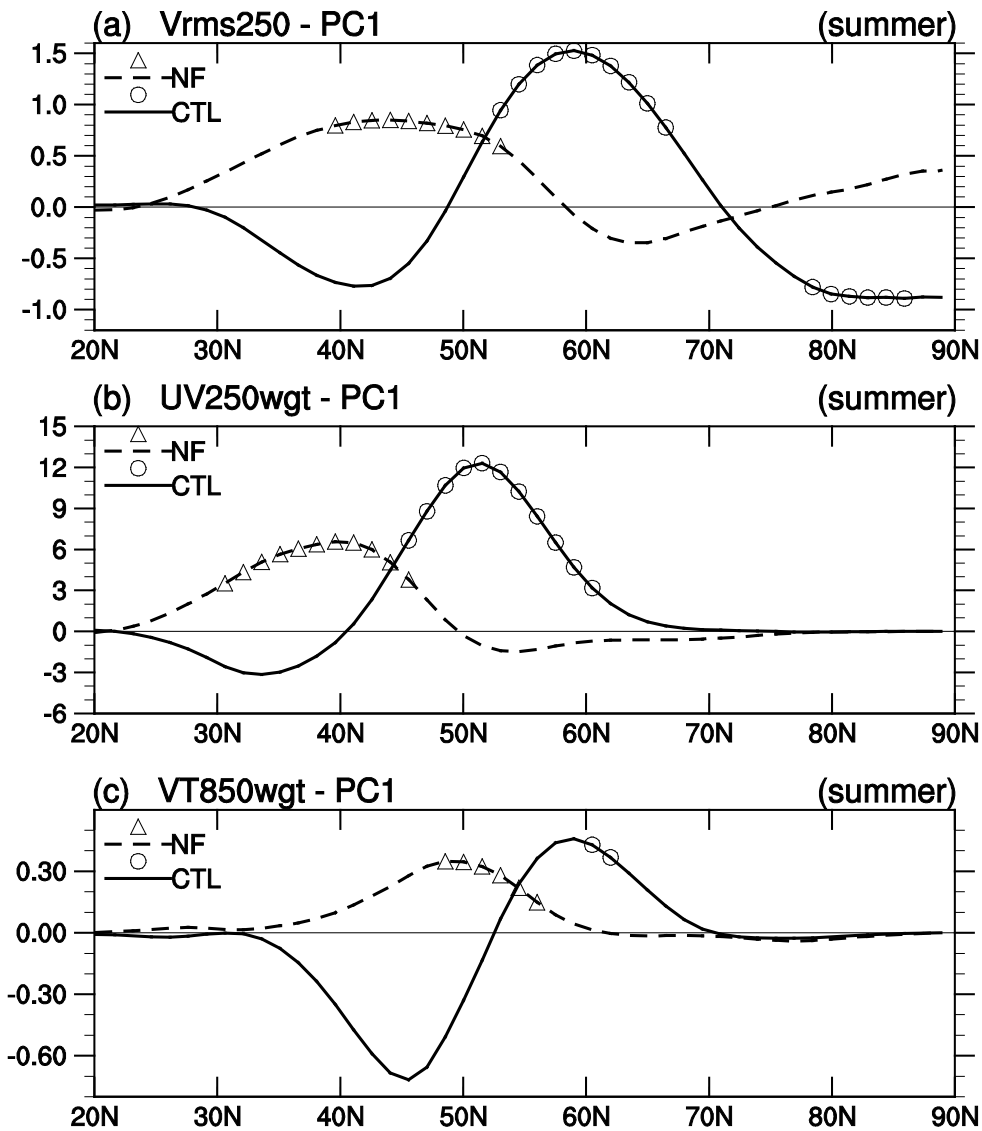


Fig. 10. As in Fig. 7a, but for the regression coefficients of zonally averaged eddy statistics in the summer hemisphere: (a) rms of 250-hPa meridional wind fluctuations ($[v'^2_{250}]^{1/2}$; m s^{-1}), (b) 250-hPa poleward eddy flux of westerly momentum ($[u'v'_{250}]$; $\text{m}^2 \text{s}^{-2}$), and (c) 850-hPa poleward eddy flux of sensible heat ($[v'T'_{850}]$; K m s^{-1}). In (b) and (c), the fluxes are multiplied by the cosine of latitude. Solid and dashed lines are for the CTL and NF experiment, respectively, with circles and triangles indicating the corresponding local correlation greater than 0.4 in magnitude.

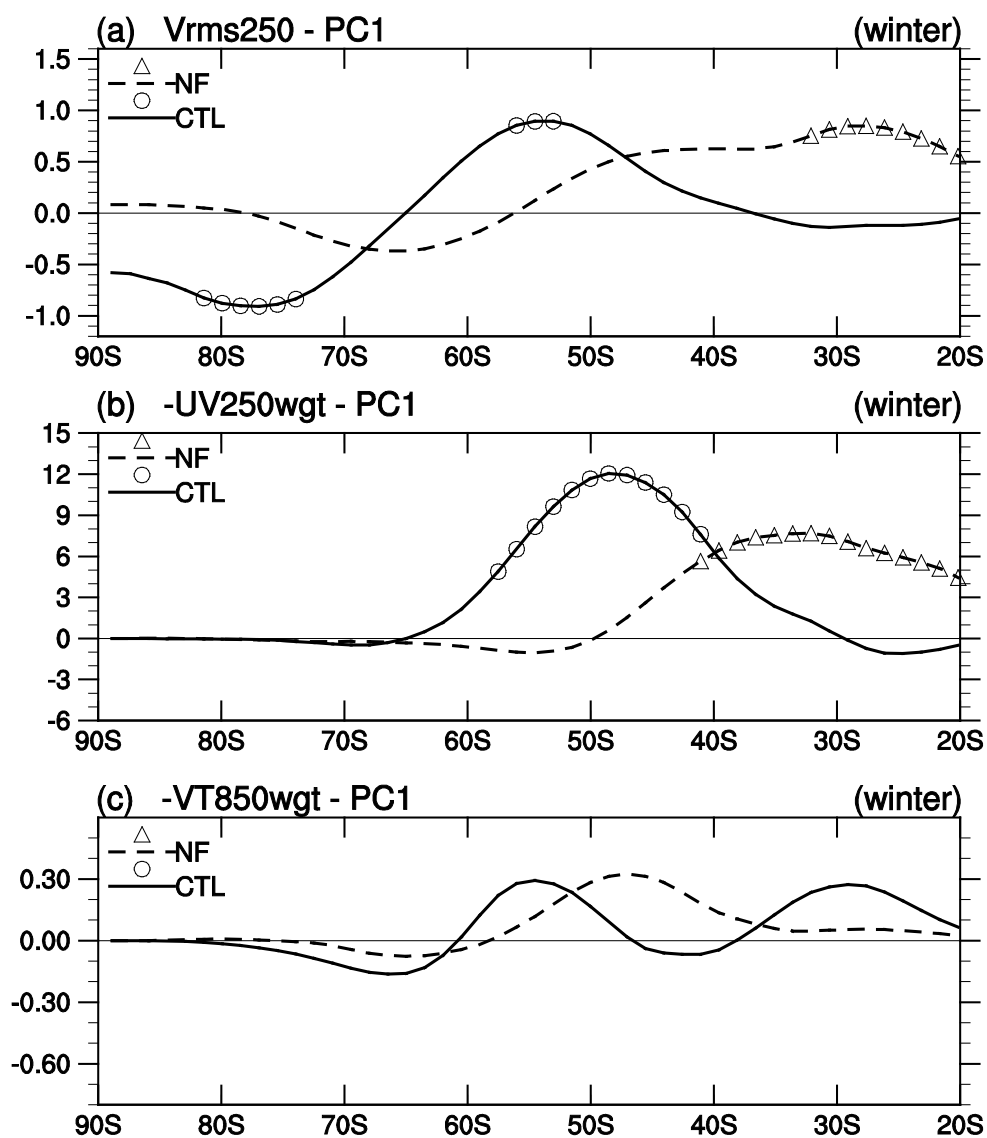


Fig. 11. As in Fig. 10, but for the winter hemisphere.

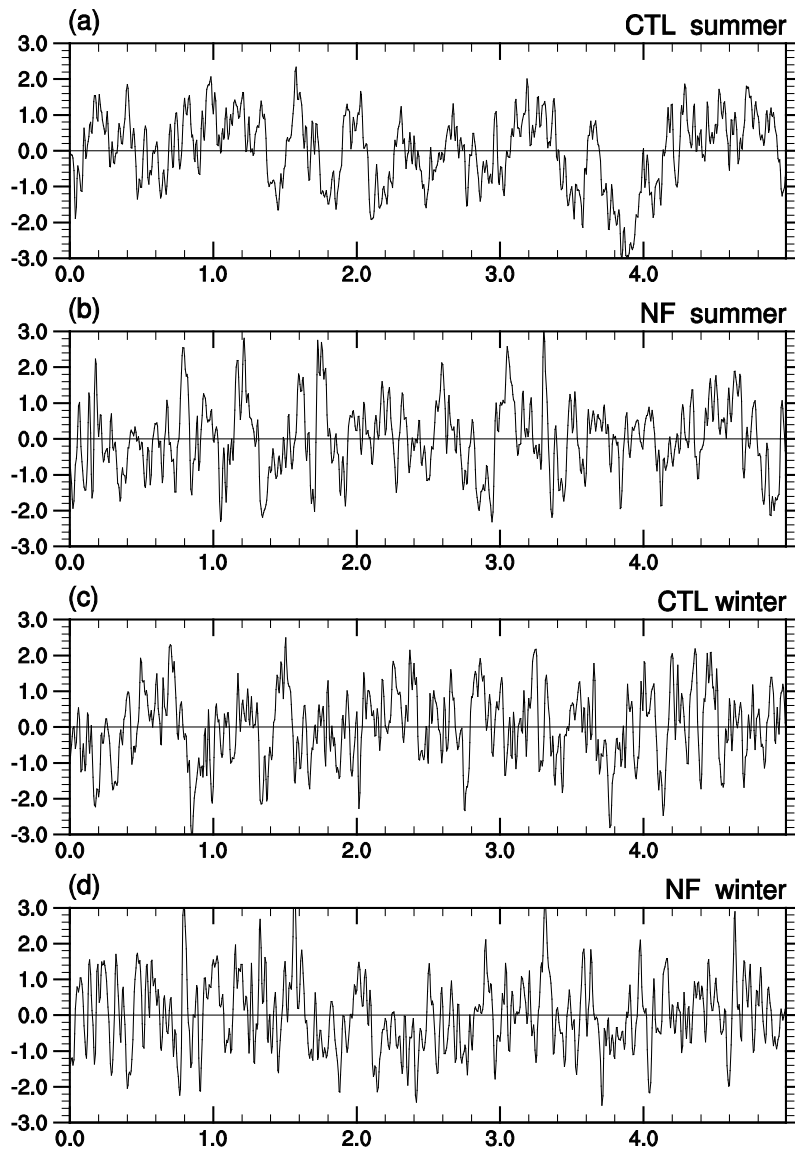


Fig. 12. Normalized principal component (PC) time series for EOF1 of 250-hPa zonal-mean zonal wind [U_{250}], or “annular mode indices”, for (a) the summer hemisphere of the CTL experiment, (b) the summer hemisphere of the NF experiment, (c) the winter hemisphere of the CTL experiment, and (d) the winter hemisphere of the NF experiment. Abscissa denotes time (year).

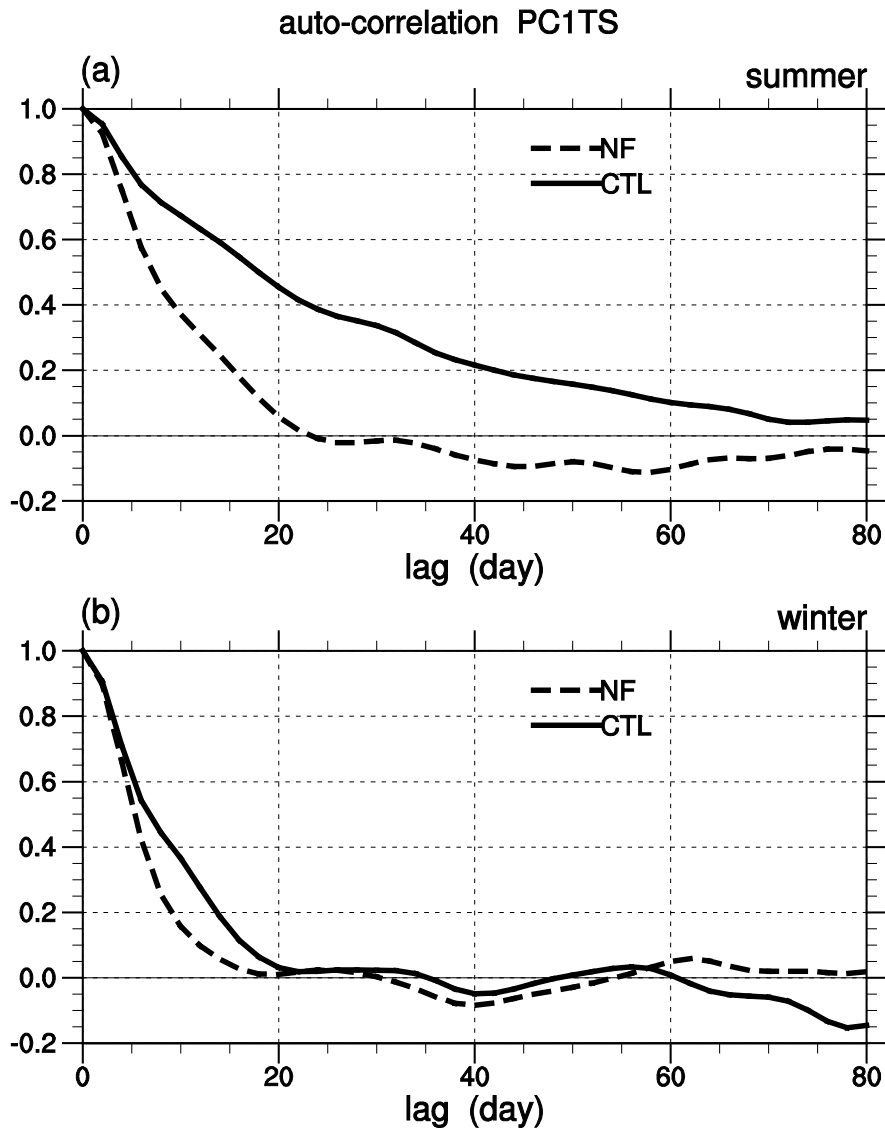


Fig. 13. Autocorrelation coefficients of the model annular mode index time series shown in Fig. 12 for the (a) summer hemisphere and (b) winter hemisphere. Solid and dashed lines denote values for the CTL and NF experiments, respectively.

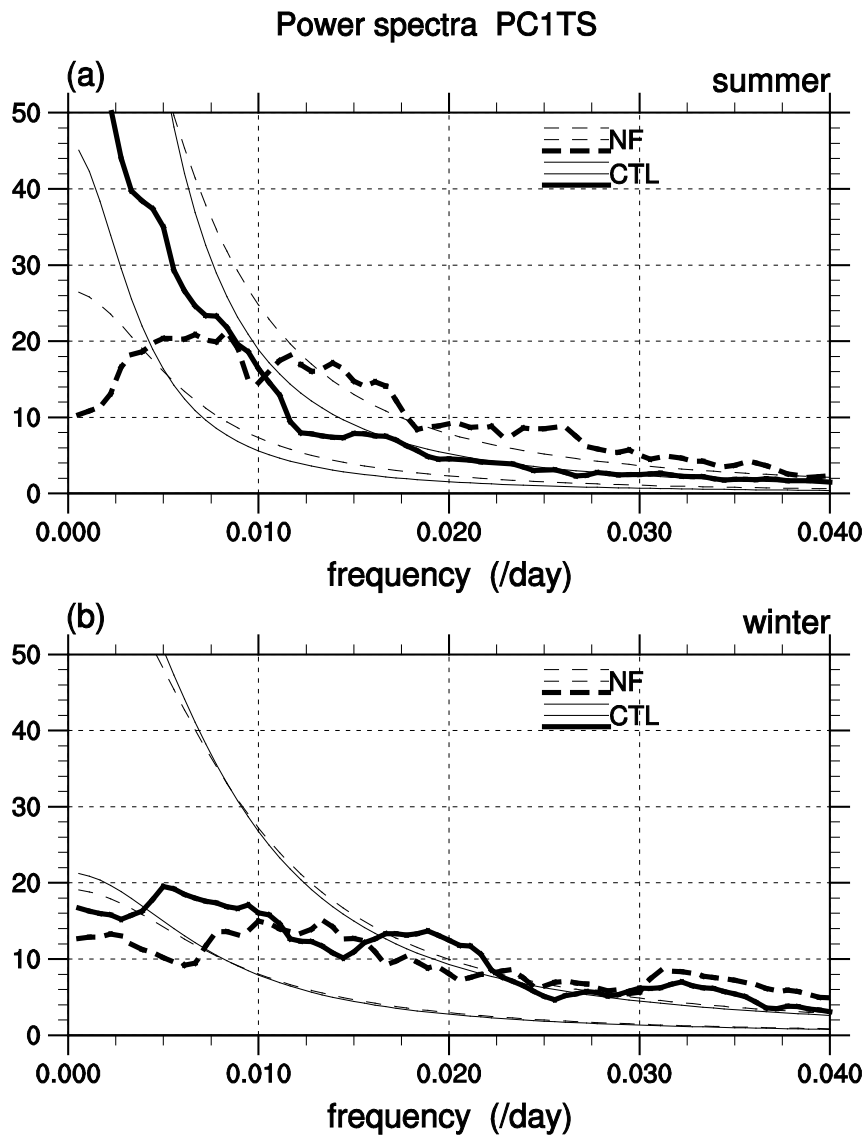


Fig. 14. As in Fig. 13, but for the power spectra. The plotted spectra have the degrees of freedom of 23.7 with a bandwidth of 0.0066 day^{-1} . Thin solid (dashed) lines indicate the 98% confidence interval for red noise for the CTL (NF) experiment.